

A model-based exploratory study of sulfur dioxide dispersions from concentrated animal feeding operations in the Southeastern United States

Jesse Winchester , Rezaul Mahmood , William Rodgers , Philip J. Silva , Nanh Lovanh , Joshua Durkee & John Loughrin

To cite this article: Jesse Winchester , Rezaul Mahmood , William Rodgers , Philip J. Silva , Nanh Lovanh , Joshua Durkee & John Loughrin (2021): A model-based exploratory study of sulfur dioxide dispersions from concentrated animal feeding operations in the Southeastern United States, Physical Geography, DOI: [10.1080/02723646.2021.1875583](https://doi.org/10.1080/02723646.2021.1875583)

To link to this article: <https://doi.org/10.1080/02723646.2021.1875583>



Published online: 21 Jan 2021.



Submit your article to this journal [↗](#)



View related articles [↗](#)



View Crossmark data [↗](#)

ARTICLE



A model-based exploratory study of sulfur dioxide dispersions from concentrated animal feeding operations in the Southeastern United States

Jesse Winchester^{a,b}, Rezaul Mahmood^c, William Rodgers^{id a,b}, Philip J. Silva^d, Nanh Lovanh^d, Joshua Durkee^a and John Loughrin^d

^aDepartment of Earth, Environmental, and Atmospheric Sciences, Bowling Green, KY, USA; ^bKentucky Climate Center, Western Kentucky University, Bowling Green, KY, USA; ^cHigh Plains Regional Climate Center, School of Natural Resources, University of Nebraska-Lincoln, Bowling Green, KY, USA; ^dUSDA-ARS, Bowling Green, Kentucky

ABSTRACT

In the Southeastern U. S. there are Concentrated Animal Feeding Operations (CAFOs) that emit a variety of gases, including SO₂. Sulfur is emitted as reduced sulfur compounds and can react in the atmosphere to produce SO₂. It is expected that the concentration and spread of SO₂ emissions from these sources would differ between wet and dry periods. In this research, SO₂ emissions from locations representing CAFOs and its dispersion over the southeastern U.S. were simulated through sensitivity experiments using the Weather Research and Forecasting-Chemistry (WRF-Chem) model. Simulations were performed for dry periods and precipitation events that occurred over western Kentucky between July 7 and 13 July 2012.

The study found that spatial coverage of SO₂ dispersion originating from these locations was reduced during precipitation events and expanded during dry periods. The average concentration of SO₂ over the study area was also higher during the breaks between precipitation events than during precipitation. The highest concentrations of SO₂ exceeding 1,000 pptv remained within close range of the emission locations for the majority of the simulations, except for when local surface wind speeds were high. Most emissions from the locations remained limited to the surface and lower levels of the atmosphere (850 mb).

ARTICLE HISTORY

Received 5 June 2019
Accepted 10 January 2021

KEYWORDS

Sulfur dioxide; livestock; dispersion; modeling; WRF-Chem; Southeastern United States

Introduction

Air pollution can be hazardous to human health, flora and fauna (Borlée et al., 2017; Khaniabadia et al., 2017; Pope & Dockery, 2006; Pope et al., 1991; Sigurdarson & Kline, 2006). Pope and Dockery (2006) noted that air pollution can adversely impacts Cardiovascular health. Borlée et al. (2017) suggested that air pollution from livestock farms negatively impacts non-farming population and their lung function. Mnatzaganian et al. (2015) found that in Maui, Hawaii, there was a significantly higher occurrences of respiratory distress in smoke-affected areas, linked to sugar cane farming.

Khan and Siddiqui (2014) also noted that respiratory system and lung functions can be impacted by higher level of sulfur dioxide (SO_2) in the air.

Pollutants such as sulfur dioxide (SO_2) are emitted from a wide variety of natural and anthropogenic sources. Natural sources include vegetation and water bodies, and anthropogenic sources include agricultural operations, industry, transportation networks, and cities (Battye et al., 2003; Cicerone & Oremland, 1988; Kleinman et al., 2002; Mosier et al., 1998). In agriculture, Concentrated Animal Feeding Operations (CAFOs) are a potentially important source of SO_2 emissions (Bunton et al., 2007). Note that the agriculture is not a major direct emissions source of SO_2 , however, it does release other reduced sulfur compounds that can photochemically oxidize to SO_2 . These may become increasingly important contributors to particulate formation as direct SO_2 emissions are reduced (Perraud et al., 2015). Since these emissions can be harmful to human health and the environment in general, it is crucial that we investigate SO_2 emissions and their dispersion under different atmospheric conditions.

This paper focuses on the spatial and temporal patterns of transport and dispersion of simulated emissions across a portion of the southeastern U.S. Specifically, these point sources represent CAFOs in western Kentucky near Bandana, Cunningham, and Boxville (Figure 1). We have selected SO_2 because it is part of a larger study. These emissions were modeled in the context of periodic convective precipitation and dry periods through the week of July 7–13, 2012 over the study area. The Weather Research and Forecasting-Chemistry (WRF-Chem) model was used to simulate emission dispersion. *This is one of the first applications of WRF-Chem for agricultural/livestock emissions and dispersion.* These simulations also provided an opportunity to assess WRF model-sensitivity and performance for this type of applications in the future. The length of the experiment is

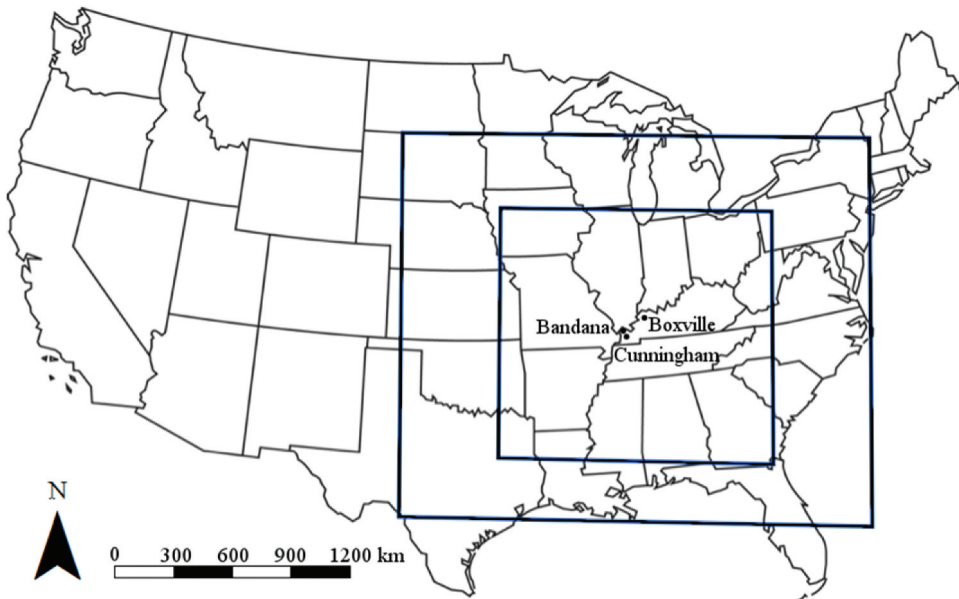


Figure 1. Inner and outer domains for the sensitivity simulations. Emission sources are labeled points within the inner domain.

generally acceptable in the air quality research involving models or observations (e. g., Loughner et al., 2011; Wang et al., 2011).

Precipitation can enhance the rate at which SO_2 is oxidized to produce sulfuric acid (H_2SO_4), a component of acid rain at high SO_2 concentrations (Menz & Seip, 2004). Hence, this study suggests that the presence of precipitation over the emission locations would result in changes to atmospheric concentration of SO_2 in their vicinity and the geographic dispersion of emissions was expected to change during precipitation in comparison to drier conditions.

Previous air pollution studies include global-scale simulations of greenhouse gas concentrations, regional-scale simulations of surface emissions and transport (Jiang et al., 2010), and smaller-scale urban emission studies focused on temporal persistence and effects on the surrounding area (Jiang & Zhao, 2008; Karl et al., 2009; Kleinman et al., 2002; Tie et al., 2007). *Compared to these studies, a limited number have focused on anthropogenic emissions from rural and agricultural environments and, in particular, from CAFOs* (Loughrin et al., 2011; Quintanar et al., 2013). These research suggest that the impacts of CAFOs on air quality warrant attention due to the nearby human settlements and inhabitants. and provided further motivation for the current study.

The results of the present research provide insight into the short-term emissions from CAFOs and their dispersion. This may also offer a framework within which future CAFO emission and dispersion studies at a similar scale can be performed for other locations. In the following sections this paper provides a literature review, brief assessment of the research questions, and methodology of the research project, followed by the results and conclusions. Components of the methodology include descriptions of the extent of the study area, event selection process, data and variables, modeling steps, and analysis. This paper concludes with a summary of the overall findings as well as statements explaining the significance and justification of the selected research topic.

Although this study verified precipitation amounts simulated by the model with observed data, a limitation of this is that we did not have observed SO_2 data for the study periods for such verification. However, we have compared simulated SO_2 with other observed studies to ensure that the simulated values are satisfactory (e.g. Loughner et al., 2011).

Background

A facility to qualify as an Animal Feeding Operation (AFO), must have animals in a concentrated area for at least 45 days of a given year. Animals include hogs, cattle, chickens, hens, and pullets. There are over 400,000 of these operations across the U.S. [United States Department of Agriculture [USDA], 2013]. The classification of an AFO as a CAFO depends on the animal species and the number of animals in a facility (Environmental Protection Agency [EPA], 2014). Different types of CAFOs, in terms of animals, are distributed across the U.S. in various patterns. For example, pig operations are concentrated in the Midwest and eastern North Carolina, while chicken operations occur in clusters scattered throughout the Southeastern US (National Research Council, 2003).

There are several gases/pollutants emit from CAFOs. These include CH_4 , CO_2 , N_2O , NH_3 , hydrogen sulfide (H_2S), and SO_2 (Bunton et al., 2007). In addition to gaseous

emissions, others such as volatile organic compounds (VOCs) and particulate matter can also be found (Ni et al., 2012; Winkel et al., 2015; Zhang et al., 2019). Particulate matter emitted from CAFOs can be composed of a complicated mix of inorganic, organic, and biological components.

Particulate matter that originates from CAFOs can cause respiratory problems, such as asthma, and can occur in human populations in the vicinity of these operations (Sigurdarson & Kline, 2006). CAFO emissions can also produce secondary particulate matter (aerosol that forms from atmospheric chemical reactions). Ammonia is known to contribute to this end and it is suspected that sulfur and VOC compounds may as well. As noted above, CAFOs emit reduced sulfur compounds that include H_2S and organic analogues such as dimethylsulfide (DMS) and methanethiol, which can react in the atmosphere to produce SO_2 and other sulfur species (Rumsey & Aneja, 2009). Feilberg et al. (2017) correctly noted that H_2S from agricultural sources is generally not included in sulfur emission estimates although it is a major sulfur compound emitted from livestock production. They have also found that livestock farming, particularly pig production, is a major agricultural source of sulfur in Denmark. It is well-known that H_2S and OH reacts in the atmosphere and has an estimated lifespan of 2.5 days (Feilberg et al., 2017). On the other hand, the atmospheric lifespan of SO_2 can be 4 to 48 h (Feilberg et al., 2017). This also suggests that conversion of H_2S to aerosol sulfate can occur over a short period of time (Feilberg et al., 2017). In addition, the chemical characteristics of H_2S is different from SO_2 especially due to a much lower water uptake of H_2S (and can have implications in simulations of dispersions if we have considered H_2S).

Global and large-scale air quality simulations are useful for obtaining the big picture of emission rates, atmospheric transport and persistence (e.g. Chen et al., 2019; Guenther et al., 2006; Niemeier et al., 2020). Emission sources in these studies are almost always areal in nature due to their large spatial scope. In addition, low spatial resolution does not allow emissions from point sources, such as individual urban plumes, to be resolved. Specific applications also include present-day assessments of emissions from varying land cover types. For example, isoprene emission factors from several vegetation species have been modeled across the globe using MEGAN (Guenther et al., 2006).

Air quality research with a regional and local focus provides smaller-scale details. Examples include studies over western and central Europe (Kim et al., 2011), the southeastern U.S. (Chuang et al., 2011), the northeastern U.S. (Ntelekos et al., 2009; Wilczak et al., 2006) and along the West Coast (Bernstein et al., 2012). *The present study provides an example of both farm and regional-scale assessment SO_2 emission and dispersion from several CAFOs in Western Kentucky.* It is one of the few modeling studies that focuses on agricultural SO_2 emissions. While SO_2 is not the major sulfur component from agricultural sources, this basic optimization must be performed prior to taking more complicated steps of looking at reduced sulfur compounds and adding their chemistry to the models to produce sulfur products downwind. Future experiments in this area will add in the chemistry of reduced sulfur compounds. The two most important would be H_2S because of its high concentration in agricultural source emissions and DMS because of its potential importance in producing secondary aerosols.

Methodology

The WRF-Chem model and experimental set-up

The Weather Research and Forecasting model with Chemistry (WRF-Chem) was developed by the National Center for Atmospheric Research [National Center for Atmospheric Research [NCAR] 2013] and has been used in a number of air quality related studies (Bernstein et al., 2012; Chapman et al., 2009; Jiang et al., 2010; Jiang & Zhao, 2008; Lee et al., 2011; Lin et al., 2010; Loughner et al., 2011; Ntelekos et al., 2009; Saide et al., 2011, 2011; Wang et al., 2010; Wu et al., 2011; Yerramilli et al., 2009; Zhang et al., 2010). WRF-Chem version 3.4.1, released in August 2012, was used to perform the simulations for this research. The simulations used North American Regional Reanalysis A (NARR-A) data produced by the National Centers for Environmental Prediction (NCEP) and distributed via the National Operation Model Archive and Distribution System (NOMADS) (Mesinger et al., 2006). The data have a horizontal resolution of 32 km and were prepared at three-hour intervals (00, 03, 06, 09, 12, 15, 18, and 21 UTC). Variables such as geopotential height, specific humidity, cloud water, mixing ratios, and wind vectors were available for 29 pressure levels.

A number of variables were provided at specific heights above the surface, including temperature, specific humidity, and pressure at 2, 10, and 30 m; potential temperature and horizontal wind vectors at 2 and 10 m; and dew point temperature and relative humidity at 2 m above the surface. Over 30 variables were available for the near surface, including temperature, precipitation, radiation and energy fluxes, pressure, planetary boundary layer (PBL) height, vegetation cover, and albedo. Soil moisture and temperature were also included for four soil levels (0–10 cm, 10–40 cm, 40–100 cm, and 100–200 cm). Each simulation was seven days long and a total of 56 observations periods were used for each event (8 observations per day x 7 days) to model upper atmospheric, near surface, and subsurface conditions.

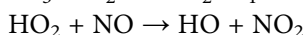
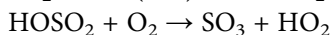
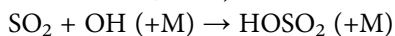
Physical parameterization schemes were selected first. There are options for the land surface model (which controls surface conditions such as energy fluxes), cumulus and convective parameterization, short-wave and long-wave radiation schemes, planetary boundary layer, and others. Parameterization schemes used are listed in Table 1. Time intervals and domain resolution were also specified in this phase.

The second phase involved the chemistry parameterization of the model. Similar to the physics options in the previous phase, various settings were available, including chemical species, photolysis, anthropogenic emissions, and biogenic emissions. To handle SO₂ chemistry, we have used Second Generation Regional Acid Deposition Model

Table 1. Parameterization schemes used for the WRF-Chem simulations.

Parameter	Scheme	Reference
Cloud microphysics	WRF Single-Moment 6-class	Hong & Lim, 2006
Longwave radiation	Rapid Radiative Transfer Model	Mlawer et al., 1997
Shortwave radiation	RRTMG Shortwave	Mlawer et al., 1997
Surface layer	MM5 Similarity	Grell et al., 1994
Land surface	Noah Land Surface Model	Chen & Dudhia, 2001
Urban surface	None	
Planetary boundary layer	Yonsei University	Hong et al., 2006
Cumulus parameterization	Kain-Fritsch	Kain & Fritsch, 1993

Mechanism (RADM2) parameterization scheme for gas and aqueous phase reactions (Gross & Stockwell, 2003). The RADM2 includes the oxidation of SO₂ by OH (Stockwell et al., 1990; Egan et al., 2014). Gaseous precursors, such as NO and OH, were included in the model using the Prep-Chem-Source 1.4 preprocessor (Freitas et al., 2011). In the model SO₂ converts via aqueous phase chemistry with OH. In the RADM2, SO₂ and NO₂ reacts with OH and are the major gas phase sources of H₂SO₄ and HNO₃, respectively (Stockwell et al., 1990). Reaction of SO₂ with OH can be shown as follows:



Stockwell et al. (1990) noted that previous experimental work (Margitan, 1984; Meagher et al., 1984; Gleason et al., 1987) verified SO₂-OH chain mechanism. In addition, RADM2 is coupled with the aerosols module the Modal Aerosol Dynamics Model for Europe (MADE) (Ackermann et al., 1998; Binkowski & Shankar, 1995) and the Secondary Organic Aerosol Model (SORGAM) (Schell et al., 2001). MADE/SORGAM predict aerosol distribution and dynamics and quantify nucleation, coagulation, condensation, and dry deposition.

The locations of the three CAFO sites selected in western Kentucky are within the inner domain and their emissions were specified. Four simulations were completed for each event, with the first simulation being the control run with no emissions change. The other three simulations included SO₂ emissions increases at these three locations and they were 10%, 20%, and 30%. Increasing emissions from the three locations isolate emissions from surrounding, allowing for identifying their particular contribution to atmospheric concentration via comparisons with the control simulation. For seven-day model simulations, each simulation took up to four actual days to complete.

This research used two domains to cover the study area. A larger area (outer domain) provided context within which the main study area (inner domain) was located (Figure 1). The outer domain spanned much of the eastern half of the U.S and had a spatial resolution of 12 km. This domain had a south-north extent ranging from 28° N, just off the Gulf Coast, to 45° N across the Great Lakes. The west-to-east extent was from -101° W in the Great Plains to -75° W along the East Coast.

The inner domain contained the southeastern U.S. with a specific focus on western Kentucky, and had a spatial resolution of 4 km. The inner domain extended from 32° N to 42° N and -96° to -81° W, spanning portions of 21 states (see Figure 1). The CAFOs in the study area primarily house pigs and chickens. Pig operations are more scattered, while chicken operations occur in concentrated areas. Of these operations, three CAFO sites were selected for the emission simulations and they were located near Cunningham, KY (36.91° N and 88.85°W), near Bandana, KY (37.16°N and 88.96°W), and near Boxville, KY (37.65° N and 87.78°W) (Figure 2). The sites represent minimal or no influence from other anthropogenic emission sources such as cities, industries and interstates.

In addition, the locations were determined by overlaying data points from the National Emissions Inventory of 2005 (NEI05) on pig CAFO maps produced by the National Research Council (2003). Several matches of CAFO locations and NEI05 data points in western Kentucky were identified. The coordinates of the corresponding NEI05 data points were obtained and used to verify the locations with satellite imagery. Again,

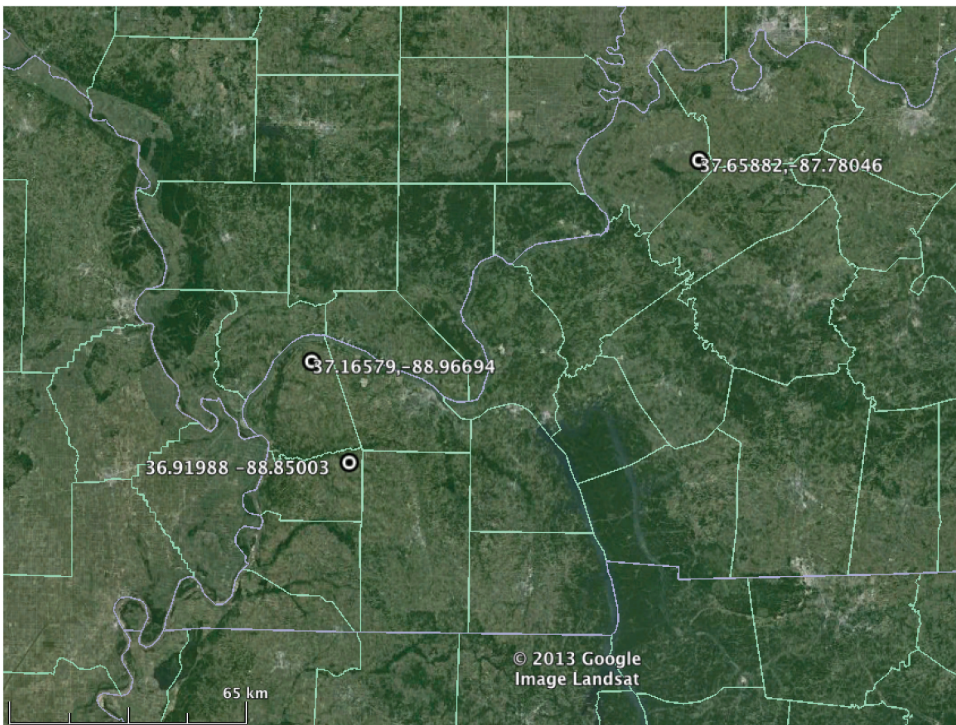


Figure 2. The locations where emissions near CAFOs in Western Kentucky were changed during the sensitivity simulations. Source: Base Map from Google Earth (2014).

this was to ensure that locations were not near any other anthropogenic sources of emissions.

Event selection

Emission simulations were performed for the period of 7–13 July 2012 which included rainy and dry periods. The process of identifying a suitable event began with the examination of observed daily precipitation maps produced by the Advanced Hydrologic Prediction Service (AHPS), a branch of the National Weather Service (NWS) (Figure 3). Over 3,000 daily maps from the AHPS precipitation image archive (2 January 2005, to 8 October 2013) were analyzed to estimate area-averaged precipitation for the inner domain.

After calculating daily area average precipitation for the inner domain for the entire map archive, they were grouped into seven-day averages. Peaks in period average precipitation were visually verified with the appropriate AHPS daily precipitation maps to check the location and characteristics of rainfall patterns. The estimated precipitation amounts during this event for the three locations selected in western Kentucky are shown in Table 2.

The following results section includes a brief discussion on synoptic condition, control simulation, and results from sensitivity experiments.

CONUS + Puerto Rico: 7/9/2012 1-Day Observed Precipitation
Valid at 7/9/2012 1200 UTC- Created 6/20/14 20:30 UTC

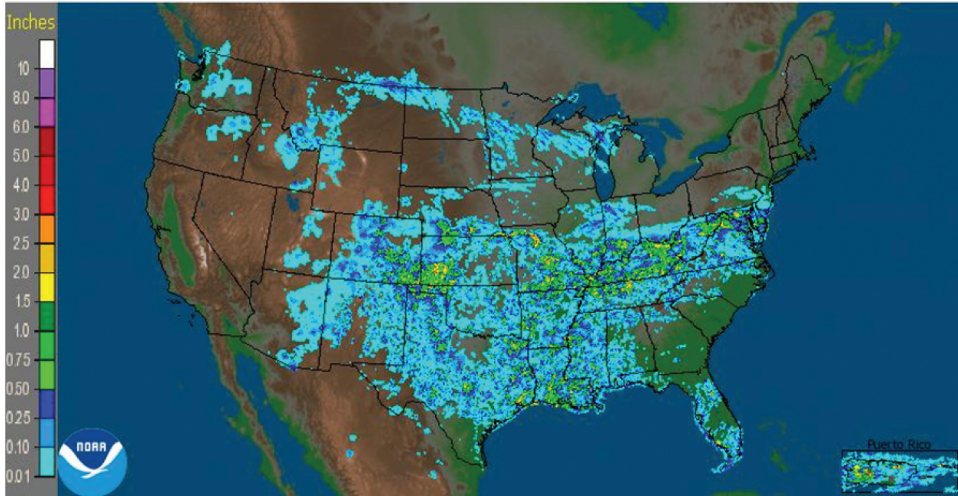


Figure 3. Daily precipitation map for the southeastern U.S. during the 24 hours ending at 1200 UTC on 9 July 2012. Source: AHPs (2012).

Table 2. Estimated precipitation amounts for the three selected locations during the July 7–13, 2012 event as derived from the AHPs daily precipitation maps (AHPs, 2012).

Location	Precipitation (mm)
Rainfall 1.8 mi NW of Bandana, KY	51.56 mm
Rainfall 2.4 mi NE of Cunningham, KY	57.40 mm
Rainfall 3.3 mi NE of Boxville, KY	14.22 mm

Results and discussions

Observed synoptic conditions

The gradual passage of a quasi-stationary front played an important role in the precipitation of July 7–13, 2012. On July 7, a cold front over the Great Lakes became stationary and started to drift slowly southward by July 8 before reaching western Kentucky on July 9 and Tennessee by July 10. The front continued over Mississippi and Alabama through July 11–12. A low-pressure center developed over the study area on July 13. Daily radar-estimated precipitation maps showed that western Kentucky received at least 1 mm of rainfall every day during this 7-day period. Most of the precipitation was observed on July 9, with some areas of western Kentucky exceeding 25 mm of rainfall coinciding with the passage of the stationary front over the study area. Doppler radar imagery also documented the passage of the stationary front. The band of rainfall associated with the front was directly over western Kentucky at 0000 UTC on July 9, or 7:00 P.M. LST. The precipitation band contained more active convective cells at 0000

UTC (7:00 P.M. CDT), likely due to daytime heating contributing to a more unstable atmosphere.

Results from the control (CTRL) simulation

The simulation of accumulated precipitation in the inner domain had a diurnal pattern, with a gradual increase from 0300 UTC to 1800 UTC each day, and a rapid increase between 1800 UTC and 0300 UTC of the next day, which coincided with the warmest part of each day. By the end of the simulation period, the inner domain had an area average accumulated precipitation of 39 mm (Figure 4(a)). The diurnal pattern was not as pronounced for accumulated precipitation in and around western Kentucky, with the first main rainfall event not occurring until late on July 8 (Figure 4(b)). Several smaller accumulations of 1–2 mm occurred from July 9 to July 11, and larger accumulation events exceeding 8 mm occurred on July 12 and 13. These resulted in a total area average accumulation of 33 mm over western Kentucky (Figure 4(b)).

Maps of accumulated precipitation for the inner domain showed that most of the precipitation in Arkansas occurred on or before July 11. This area of the highest accumulations expanded eastward into Mississippi and Tennessee on July 12 and into Alabama on July 13. Overall, the simulation produced a larger amount of precipitation in the southern half of the inner domain than in the northern half during the study period (Figure 5).

Hourly precipitation totals averaged for the inner domain better illustrated the diurnal pattern of rainfall that occurred throughout the July 7–13 period. With the exception of the first rainfall event at the end of July 7, all successive rainfall events had one or more hours exceeding 0.4 mm, with three hours during the July 8–9 event reaching or exceeding 0.6 mm (Figure 6(a)). In western Kentucky (the vicinity of the CAFOs), a larger amount of average hourly precipitation was simulated during July 8–9, compared to the entire inner domain. Additionally, a bimodal pattern in hourly precipitation was present for western Kentucky with two peaks separated by 1–3 hours (Figure 6(b)). The second peak of precipitation was much smaller than the first.

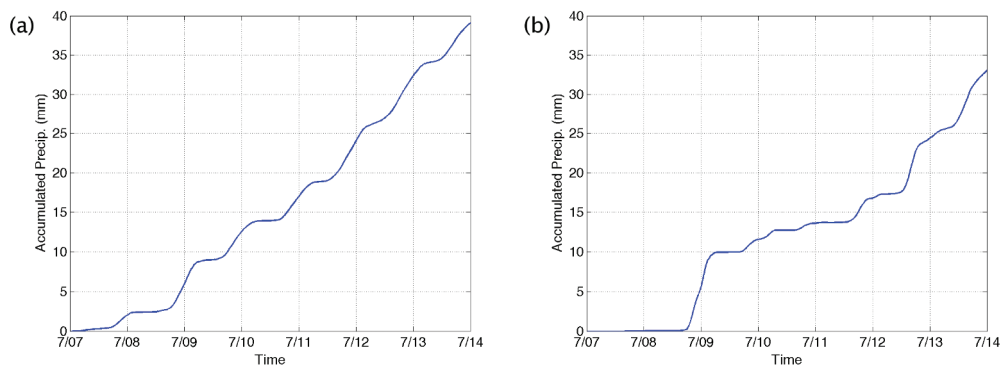


Figure 4. Simulated area average accumulated precipitation (mm) during the July 7–13, 2012 event for (a) the inner domain and (b) the vicinity of the CAFO emission points. Dates represent 0000 UTC.

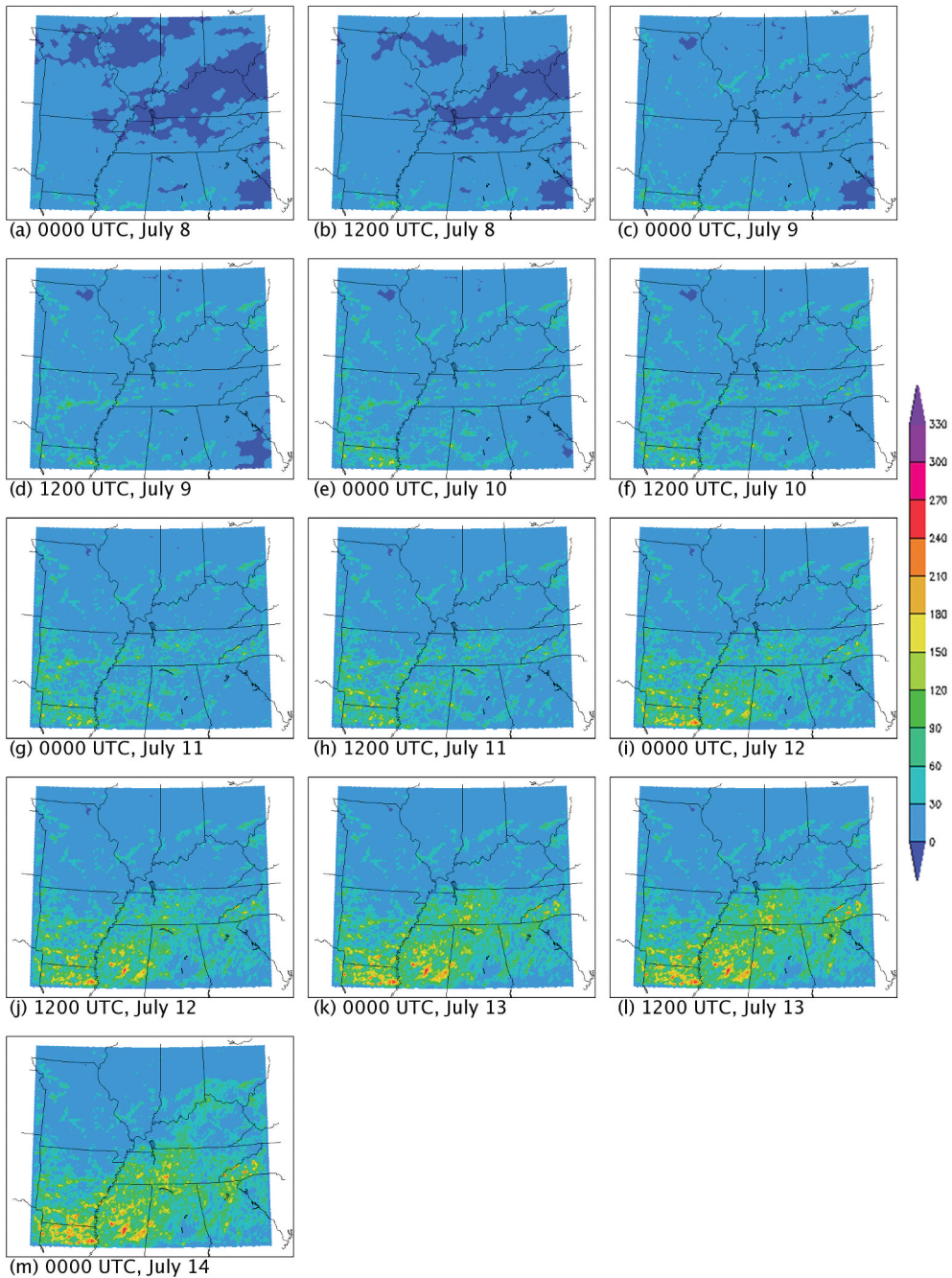


Figure 5. Inner domain accumulated precipitation (mm) starting at 0000 UTC on 7 July 2012.

Twelve-hour accumulation maps (Figure 7(a-m)) for the entire study period are shown in Figure 7(a-m). For the inner domain, most precipitation occurred in Arkansas, Mississippi, and Alabama at 0000 UTC on July 8 (Figure 7(a)). By July 9, precipitation associated with the stationary front had entered the inner domain,

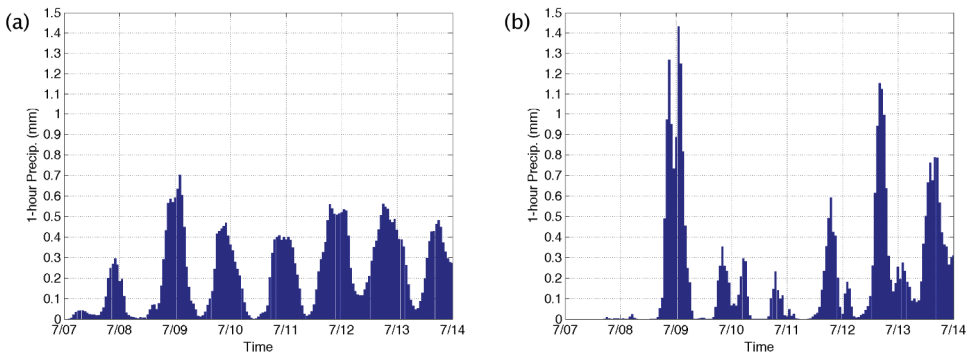


Figure 6. Area average hour precipitation totals (mm) during the July 7–13, 2012 event for (a) the inner domain and (b) the vicinity of the CAFO emission points. Dates starts at 0000 UTC.

stretching from Ohio through southern Missouri (Figure 7(c)). By 1200 UTC, precipitation passed over the western Kentucky, resulting in its highest hourly rainfall totals for the simulated period (Figure 7(d)). From July 10 to July 12, rainfall remained mostly limited to the southern half of the inner domain (Figure 7(e-j)). On July 13, the areas of higher precipitation totals progressed northward back into Kentucky (Figure 7(k)) and these persisted until the end of the simulation period.

Control precipitation and verification

Evaluation of the performance of the model, particularly with regards to precipitation, is important due to its localized nature and impacts on the results of this study. For this purpose, 24-hour simulated and accumulated precipitation were compared with the data from the Advanced Hydrologic Prediction Service (Advanced Hydrologic Prediction Service [AHPS], 2012) for each day. The comparison of simulated precipitation with AHPS data shows agreement and disagreement in terms of intensity and locational differences through the entire simulation period (Figure 8(a-e)). For example, comparisons on July 10 suggest that simulated precipitation occurred in the same areas as precipitation in the AHPS data. However, precipitation amounts were overestimated in southern Arkansas, Mississippi, and Alabama and underestimated along the Kentucky-Tennessee border (Figure 8(a-b)). On July 11, AHPS data suggest that most of the precipitation occurred in northern Alabama and south-central Tennessee, and this was also reflected in the model results. Precipitation totals were overestimated in areas south and west, including much of Mississippi and southeastern Arkansas (Figure 8(c-d)).

AHPS data suggest that July 12 precipitation generally occurred over the same locations as July 11 with comparable magnitudes. However, greater accumulations shifted farther south over Alabama and Mississippi. The model underestimated precipitation in these areas and overestimated amounts in much of Tennessee and western Kentucky (Figure 8(e-f)). Throughout the entire simulation, the general location of modeled precipitation agreed in most cases with AHPS estimates, but the amounts of precipitation were frequently over- or under-estimated.

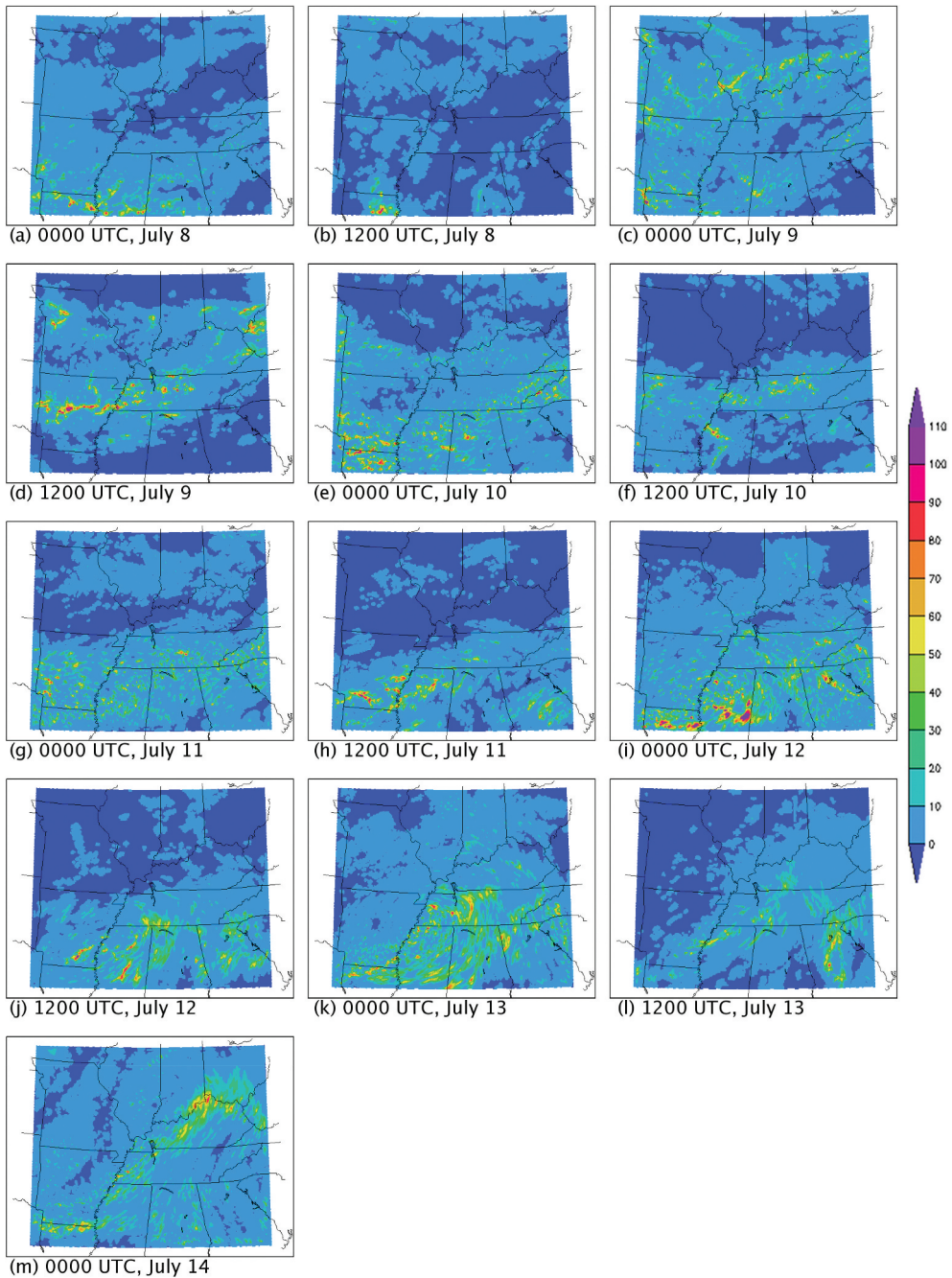


Figure 7. Inner domain 12-hour precipitation totals (mm) for the July 7–13, 2012 event.

Control simulation of SO_2

In this section, spatio-temporal distribution of SO_2 and key meteorological variables obtained from the control simulation are discussed. Horizontal wind speeds, on average

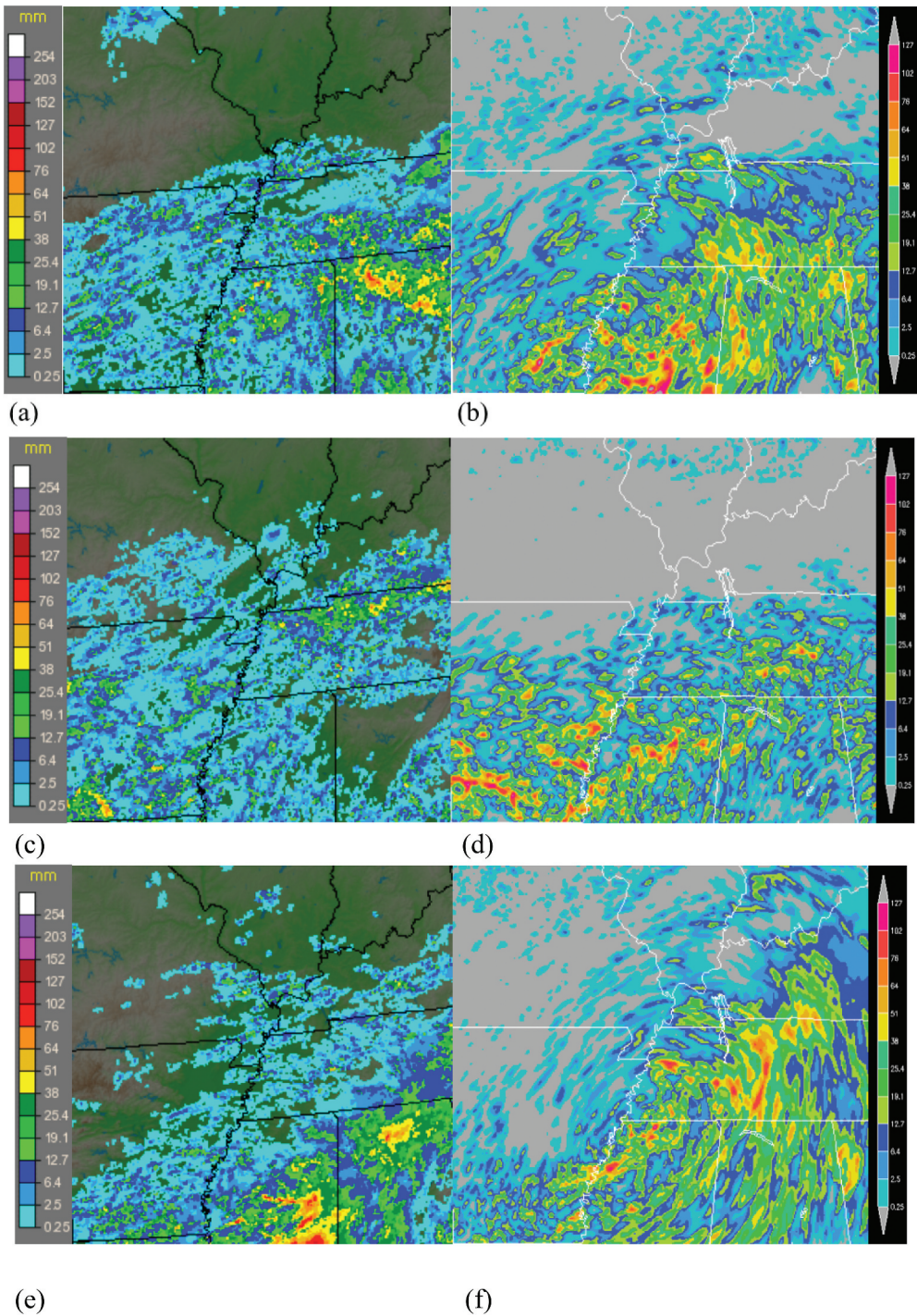


Figure 8. 24-hour accumulated precipitation (mm) over the core of the inner domain starting at 1200 UTC on: 10 July 2012 (a) from Doppler radar estimates by the AHPS (2012), (b) from the WRF-Chem control simulation, (c) like as (a) but for on July 11, (d) like (b) but for July 11, (e) like (a) but for 12 July 2012, (f) like (b) but for 12 July 2012.

for the inner domain, were the lowest at the surface and highest (10 m s^{-1} on average) aloft at the 300-mb level. Wind speed peaks at the surface appeared to coincide with the peaks in hourly precipitation. However, this comparison was less noticeable in the upper levels. For the western Kentucky area (location of emissions sources), winds were much stronger aloft (near 18 m s^{-1}). Wind speeds at all levels decreased below 5 m s^{-1} following the July 8–9 precipitation event before rebounding back to their previous speeds near the beginning of July 10. Additionally, while wind speeds at the 700 and 500-mb levels were greater than those at the surface before July 9, it decreased near equal to surface level for the rest of the period after the July 8–9 rainfall event.

A diurnal pattern in SO_2 concentrations was observed at the surface, with minima and maxima reaching near 1200 and 1800 UTC, respectively. Concentrations decreased at all levels during the stationary frontal passage and associated precipitation on July 8–9 and remained under 60 pptv for the remainder of the simulation period as rainfall continued throughout the inner domain (Figure 9(a)). The lowering of SO_2 concentrations on July 8 was more pronounced for the western Kentucky and reached below 50 pptv. SO_2 at the 300 mb level rebounded to near 70 pptv on July 11, while those at the lower level of the atmosphere remained below 40 pptv. SO_2 at the 300 mb level decreased again with the onset of more precipitation in the western Kentucky on July 12 and July 13, and concentrations at the surface, 850 mb, and 700 mb levels reached near zero (Figure 9(b)).

Results from sensitivity experiments

Area average temporal changes

In the first of the four sensitivity experiments conducted, SO_2 emissions at the three locations representing CAFOs in western Kentucky were set to the average of surrounding emissions (EXPAVG). In the subsequent simulations, the average SO_2 emissions calculated in EXPAVG were increased by 10% (EXP10), 20% (EXP20), and 30% (EXP30). At the surface for the entire inner domain, the area-averaged increase in emissions from CTRL was as much as 10 pptv before July 9, and the increase ranged between 10 and 20 pptv above CTRL in all EXP simulations for the remainder of the

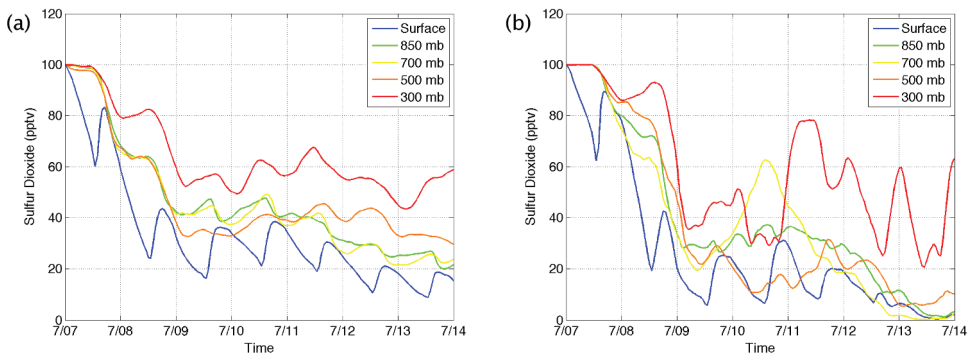


Figure 9. Area average SO_2 concentrations (pptv) during the July 7–13, 2012 event for control simulation: (a) the inner domain and (b) the vicinity of the CAFO emission points. Dates represent 0000 UTC.

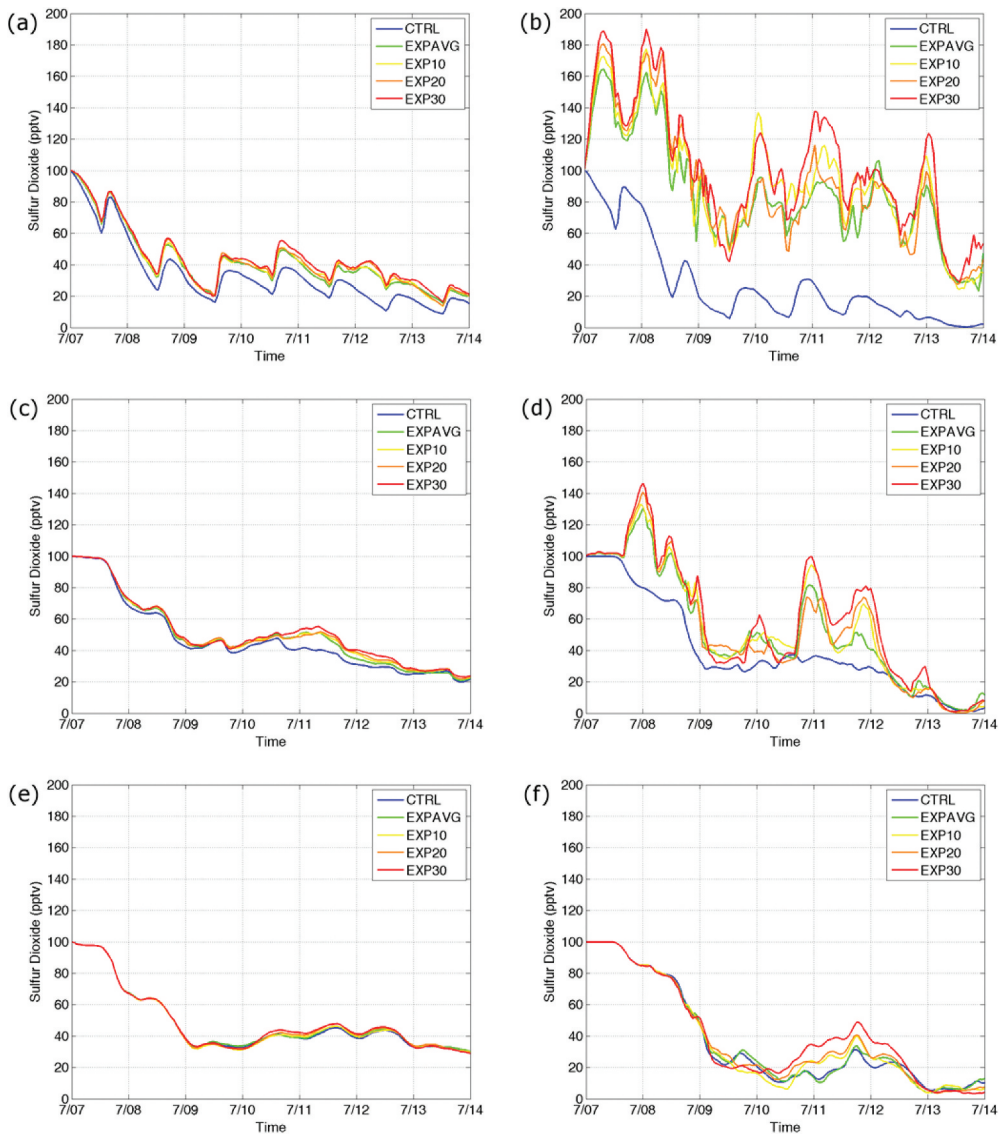


Figure 10. Area average SO_2 concentrations (pptv) at the surface for the emissions change simulations during the July 7–13, 2012 event over (a) the inner domain, (b) the vicinity of the CAFO emission sources, c) as ‘a’ but for 850 mb level, d) as ‘b’ but for 850 mb level, e) as ‘a’ but for 700 mb level, and f) as ‘b’ but for 700 mb level.

period (Figure 10(a)). Near to the emissions change locations, the increase in SO_2 from CTRL was much greater in all EXP simulations, with area-averaged increases of up to 110 pptv from CTRL occurring at 0000 UTC on several days (Figure 10(b)). For most of the simulation period, EXPAVG had the lowest and EXP30 had the highest concentrations. However, there were brief fluctuations of these concentration on July 9 and July 12 (Figure 10(b)). These fluctuations coincided with increased precipitation in

western Kentucky on these days (*cf.*, Thornton et al., 1997; Tu et al., 2004; Wang et al., 2011).

At the 850 mb level, there was less of a difference between CTRL and the emissions change simulations than near the surface, and the diurnal pattern of concentrations was less pronounced across the inner domain (Figure 10(c)). The difference between EXP30 and CTRL remained at 10 pptv or less until July 10 and then increased to near 20 pptv, with EXPAVG, EXP10, and EXP20 having smaller changes from CTRL. The area-averaged concentrations of SO₂ for the area near the emissions change locations were again higher than those for the entire inner domain, reaching as much as 70 pptv above CTRL for the EXP30 simulation at 0000 UTC on July 8 and July 11 (Figure 10(d)).

There were lower differences between the emissions change simulations and CTRL above the 850 mb level. Over the entire inner domain, there was an average increase in SO₂ concentrations of up to 5 pptv on July 10 and 11 between all simulations, but the average concentration between them matched closely during the rest of the period at the 700 mb (Figure 10(e)), 500 mb (not shown), and 300 mb levels (not shown). For the area in the vicinity of the emissions change locations, there was little difference in SO₂ concentrations between simulations at the 700 mb level (Figure 10(f)) and higher until July 9. At the 700 mb level, the local area-averaged concentration for CTRL was up to 20 pptv higher than those for the emissions increase simulations, but there was little difference between all simulations again by 1200 UTC on July 10 (Figure 10(f)). The most area-averaged changes in SO₂ at the 500 mb level occurred between 1200 UTC on July 10 and 1200 UTC on July 12, with concentrations in the EXP30 simulations being up to 20 pptv greater than CTRL.

Spatial changes

At the surface at 0000 UTC on July 8, the largest increases of SO₂ concentrations from CTRL in the EXP simulations were at least 1,000 pptv near the emissions change locations representing the CAFOs in western Kentucky (Figures 11 and 12). These increased emissions had spread to the north of their sources into Indiana and Illinois due to southerly winds, with the difference in concentrations from CTRL decreasing rapidly with distance. Changes from CTRL at the 850 mb level were similar to those at the surface in all EXP simulations (Figures 11 and 12).

Figure 13(a-h) shows dispersion and concentration of SO₂ at the surface and at 850 mb level. By 1200 UTC on July 8 at the surface, the area of increased SO₂ concentrations had expanded farther toward the north (Figure 13(a)). The increases were greater than 100 pptv compared to CTRL and were spreading into southern Illinois and Indiana in all EXP simulations at the surface (Figure 13(a,c,e,g)). Another area of SO₂ increase of up to 900 pptv appeared along the northeastern boundary of the inner domain. Increases of up to 300 pptv at the 850 mb level were also present in the same areas as those at the surface, and extended along the border of Kentucky and Indiana and into western Ohio (Figure 13(b,d,f,h)).

Emissions began to disperse toward the south into Tennessee with northerly winds at 0000 UTC on July 9 near the surface (not shown). Increased concentrations were mostly restricted to narrow bands at the surface, while those at the 850 mb level were more widespread, exceeding 900 pptv in EXP30-CTRL, 700 pptv in EXP20-CTRL, and 500 pptv in EXP10-CTRL. By 1200 UTC (Figure 14(a-h)), emissions continued to disperse

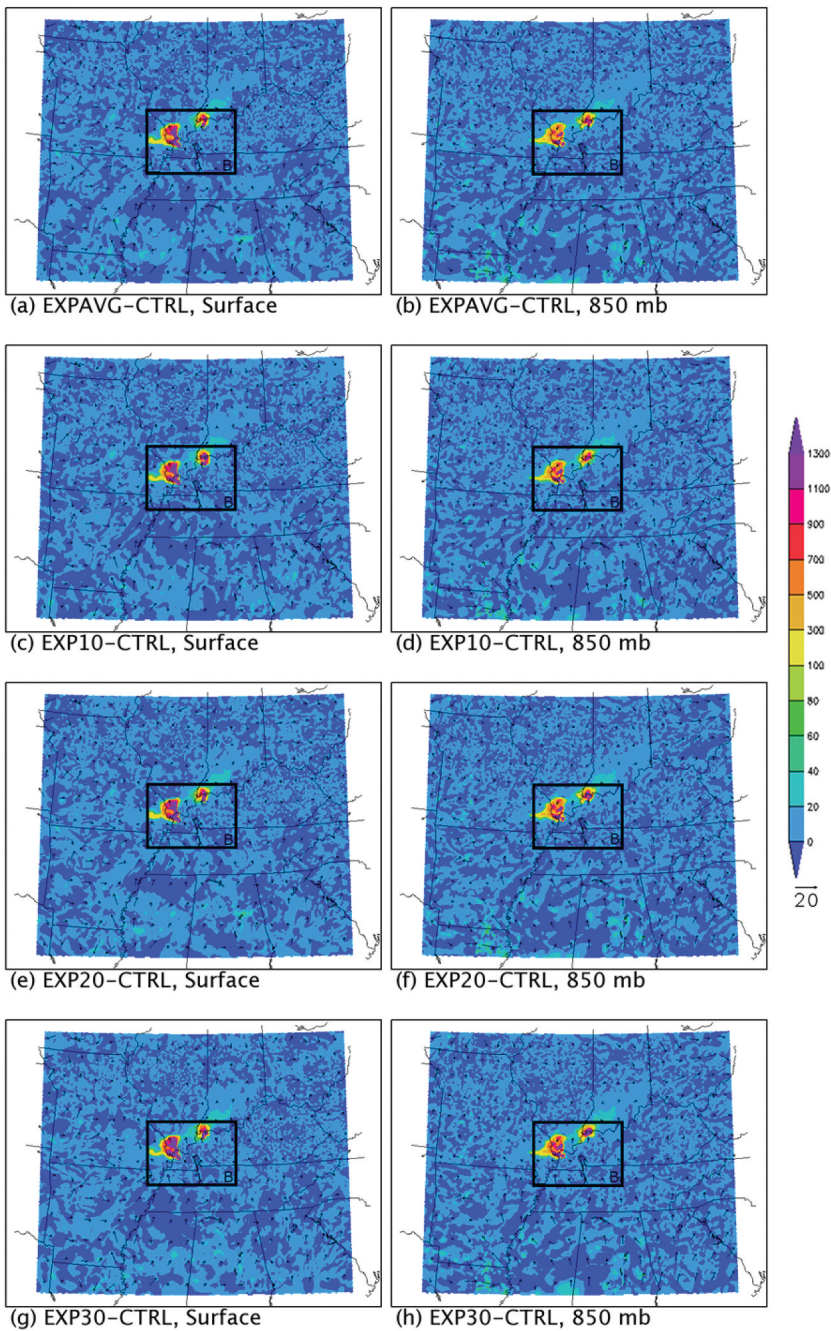


Figure 11. Changes in SO₂ concentrations (pptv) from CTRL and horizontal wind vectors (m s⁻¹) at the surface and 850 mb levels within the inner domain for each of the emissions increase simulations at 0000 UTC on 8 July 2012. The areas enclosed by box B are expanded in Figure 12.

southward in all EXP simulations, and increased SO₂ concentrations were less widespread in EXP30 than in the other simulations. At the 850 mb level, there was small

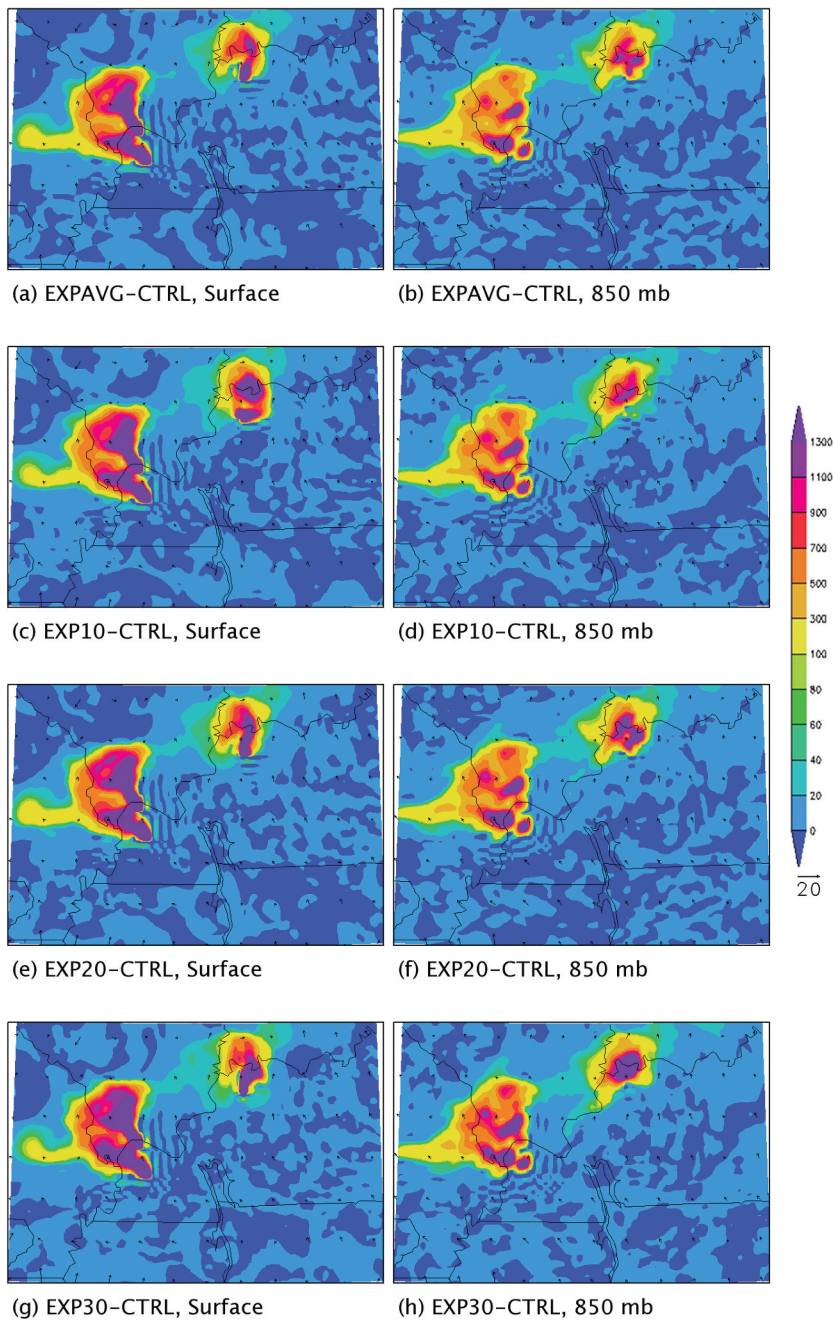


Figure 12. Changes in SO_2 concentrations (pptv) from CTRL and horizontal wind vectors (m s^{-1}) at the surface and 850 mb levels within box B from Figure 11.

increase in concentrations for EXP30-CTRL. However, increases of up to 300 pptv for EXP20-CTRL and up to 60 pptv for EXP10-CTRL and EXPAVG-CTRL were also found (Figure 14(b,d,f,h)).

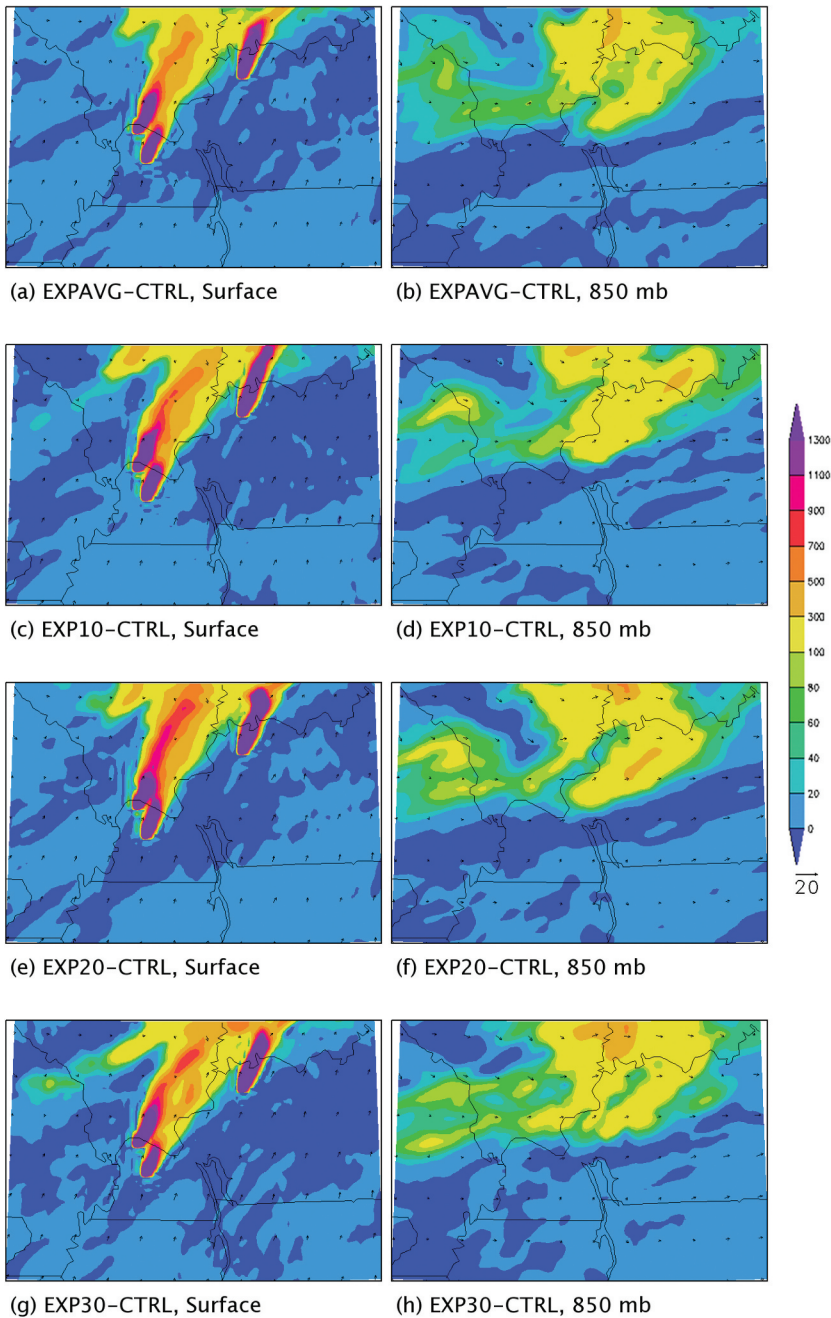


Figure 13. Changes in SO_2 concentrations (pptv) from CTRL and horizontal wind vectors (m s^{-1}) at the surface and 850 mb levels at 1200 UTC on 8 July 2012.

At 0000 UTC on July 10, the CAFO emitted SO_2 began to travel toward the south-southwest. While SO_2 concentrations exceeding 700 pptv above CTRL remained limited

to the emission locations, concentrations up to 500 pptv spread into parts of eastern Missouri from the western emission locations, and those from the location to the east continued to travel toward the south into the Land Between the Lakes area in EXPAVG and EXP10. In EXP20 and EXP30, localized concentrations around the emission locations were higher, but the extent of the spatial dispersion was more limited. For the area near the emission sources at the 850 mb level, increased concentrations were transporting toward the south-southwest, but were less widespread than those at the surface.

Surface emissions at 1200 UTC on July 10 remained limited to western Kentucky and southern Illinois in EXPAVG and EXP10. In EXP20 and EXP30, emissions traveled more toward the west into eastern Missouri with a larger area of SO₂ concentrations up to 300 pptv above CTRL. At the 850 mb level, there was a band of increased concentrations to the west of the emission locations in eastern Missouri and northern Arkansas. The location of the greatest increase within the band differed between simulations, with the greatest increase exceeding 100 pptv above CTRL over eastern Missouri in EXP10, across the state boundary between Missouri and Arkansas in EXPAVG, and over northern Arkansas only in EXP20 and EXP30.

Emissions at the surface transported toward the west from all locations at 0000 UTC and 1200 UTC on July 11, with SO₂ concentrations exceeding 100 pptv above CTRL in southern Illinois and southeastern Missouri in all EXP simulations. In EXP20 and EXP30, emissions also entered far northeastern Arkansas. At the 850 mb level, SO₂ concentrations in all EXP simulations were more widespread than those at the surface, with increased emissions transported farther into northeastern Arkansas in all cases. The earlier emissions to the east had drifted southwest into eastern Kentucky, western Virginia, and northeastern Tennessee at both the surface and 850 mb levels, with the highest increases from CTRL continuing to exceed 100 pptv.

Surface emission dispersion turned more toward the north and northwest from their sources at 0000 UTC on July 12. Emissions in EXPAVG were limited to southern Illinois, but those in EXP10, EXP20, and EXP30 also entered southeastern Missouri. There were more differences between emission sources at the 850 mb level, as only emissions from the easternmost location were apparent in EXPAVG and EXP10. Emissions originating from the western locations were more visible in EXP20 and EXP30 as concentrations exceeding 100 pptv above CTRL and spreading through the southeastern Missouri.

Emissions transported farther to the north and northwest into Illinois and Missouri at 1200 UTC on July 12 ([Figure 15\(a-h\)](#)), with concentrations exceeding 80 pptv above CTRL in these areas and in all EXP simulations ([Figure 15\(a,c,e,g\)](#)). This expansion of increased SO₂ concentrations from CTRL is likely due, in part, to precipitation moving southward from the emission locations at this time. There was also an increase of up to 300 pptv above CTRL in Ohio and part of Indiana coincident with the northern boundary of the inner domain, and it is uncertain if this was related to the emissions. At the 850 mb level, the counterclockwise rotation of winds caused emissions to turn toward the southwest and moved across Missouri with smaller increases of concentration in EXP20 and EXP30, compared to CTRL ([Figure 15\(b,d,f,h\)](#)).

At 0000 UTC on July 13, the emissions plume extended toward the west into southern Illinois and southeastern Missouri at the surface in all EXP simulations. Additionally, emissions remained more spatially compact than at earlier times, with high

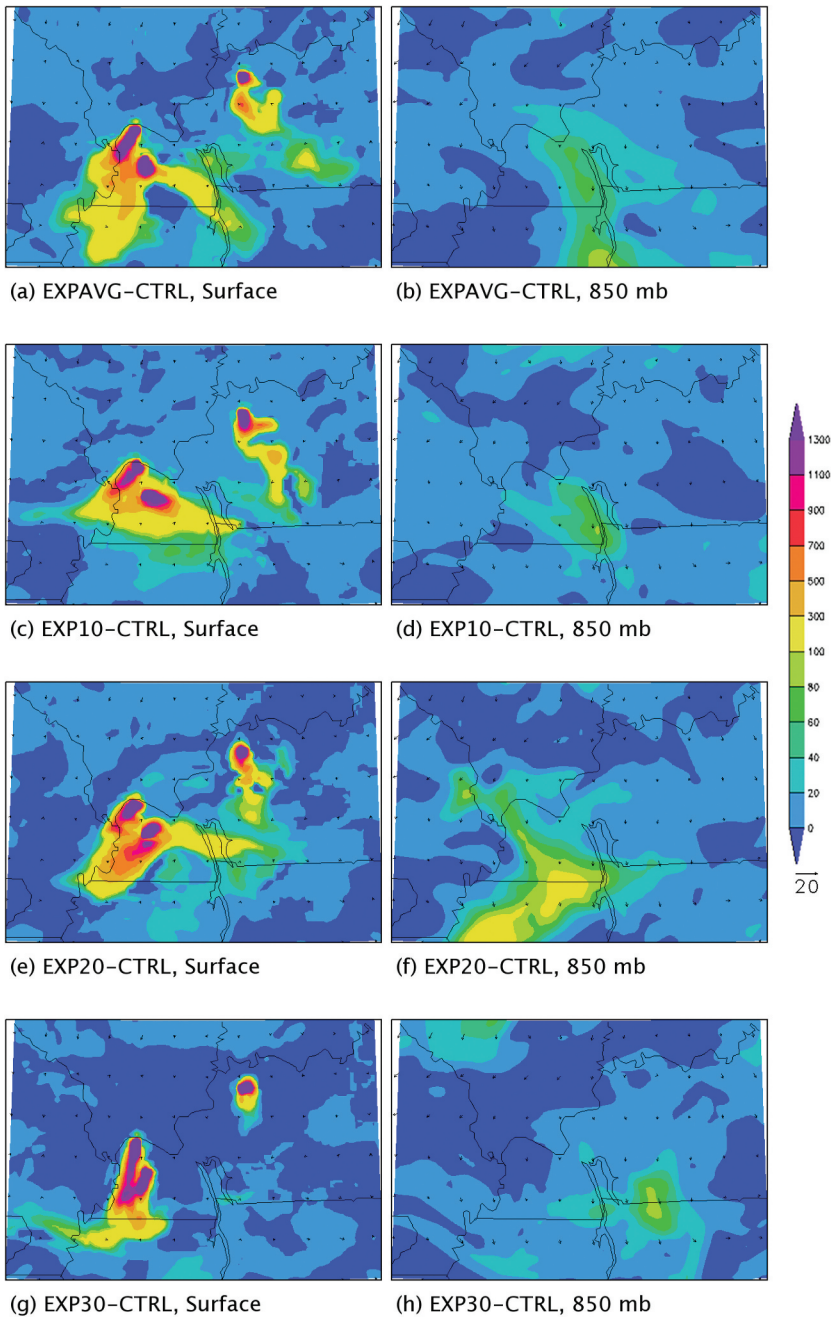


Figure 14. Changes in SO_2 concentrations (pptv) from CTRL and horizontal wind vectors (m s^{-1}) at the surface and 850 mb levels at 1200 UTC on 9 July 2012.

concentrations forming narrow bands. The highest concentrations exceeding 1,000 pptv above CTRL also extended farther from their sources than previously.

By 1200 UTC on July 13 and through 0000 UTC on July 14, emissions did not extend very far from their sources at the surface, as SO₂ concentrations quickly lowered with distance. At the 850 mb level, the emissions around their sources were completely absent, but the prior emissions to the west were still present, reaching up to 300–500 pptv greater than CTRL, in areas oriented along the northerly flow of wind.

Aerial extent of SO₂ dispersion

The spatial extent of increased SO₂ concentrations around the emissions locations varied throughout the seven-day period. In this section, the changes in the size of area affected by increased SO₂ concentrations during the different experimental simulations and the relation to precipitation are discussed. In the area close to the three specific emission locations in the western Kentucky, the size of increased concentrations of >100 pptv over CTRL was as high as about 10,000 km² in all simulations prior to increased precipitation on each day. The size decreased during each precipitation event followed by expansions of area after the end of precipitation (Figure 16(a)) (*cf.*, Thornton et al., 1997; Tu et al., 2004; Wang et al., 2011).

In the area near the changed emission locations, at the 850 mb level, the area of SO₂ concentrations >100 pptv above CTRL increased to between 9,000 and 11,000 km² in all EXP simulations on July 8. They decreased to near zero after the precipitation early on July 9 with the exception of EXP20. The two peaks in the area of increased SO₂ were reflected, to an extent, in the CAFO area on July 10 and 11, and it disappeared after the larger amount of precipitation on July 12 (Figure 16(b)). There was little to no area with increases in SO₂ concentrations at least 100 pptv for EXP-CTRL above the 850 mb level.

Discussions

The WRF-Chem applications and simulated of SO₂ dispersion over a geographic area under wet and dry atmospheric conditions generally agreed with our conceptual understanding. Results showed that with wet and dry conditions SO₂ concentrations were lower and higher, respectively. In addition, simulations suggest background SO₂ concentrations were greater at higher levels than those closer to the surface and is linked to reaction between SO₂ and precipitation in the lower levels. It is found that increased emissions from the CAFOs resulted in wider dispersion except during higher wind speeds.

As noted previously, that there is lack of studies focusing on applications of the WRF-Chem for agricultural SO₂ emissions. However, a study by Bela et al. (2016) showed lower concentration of SO₂ at lower level of the atmosphere. This is somewhat similar to our control simulations for this study (Winchester, 2015). In an observational data-based study Thornton et al. (1996) found increasing SO₂ level with increasing height over the north Pacific. Tu et al. (2004) investigated long-range transport of SO₂ from the east Asia to the central North Pacific. They have found SO₂-enriched layers above the boundary layer with low water vapor. Based on additional analysis of data they suggested that cloud processes helped to remove SO₂ and cloud free condition can assist SO₂ dispersion to longer distance (Tu et al., 2004). Our study also found similar results where dry conditions helped dispersion of SO₂ to longer distances while precipitation restricted dispersion.

Loughner et al. (2011) used WRF model to simulate meteorological data which were fed to Community Multi-Scale Air Quality (CMAQ) to simulate pollutant transport and

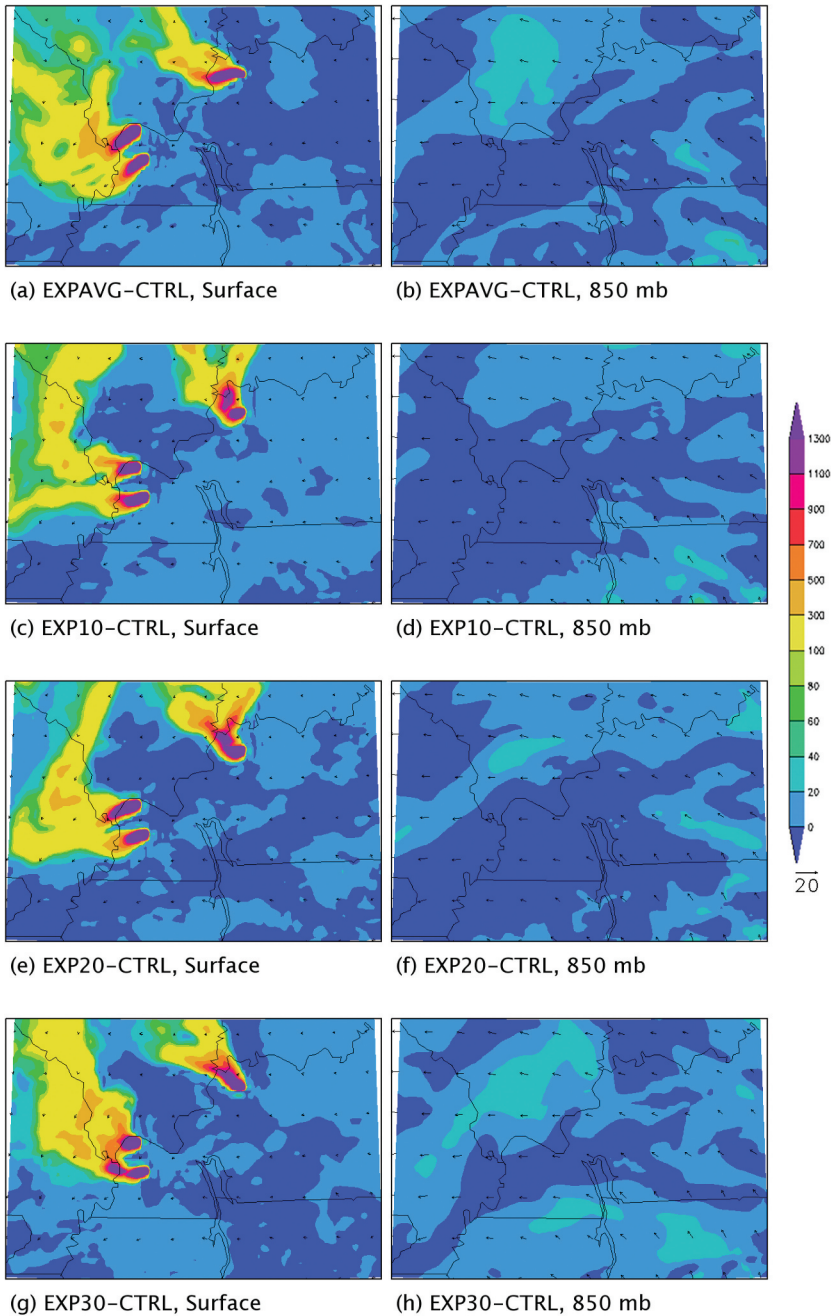


Figure 15. Changes in SO_2 concentrations (pptv) from CTRL and horizontal wind vectors (m s^{-1}) at the surface and 850 mb levels at 1200 UTC on 12 July 2012.

conversion of SO_2 to sulfate in the Washington DC-Baltimore metropolitan area. They have found that increased model resolution improved simulated results compared to observations. These simulations also show an increased rate of oxidation of SO_2 to sulfate

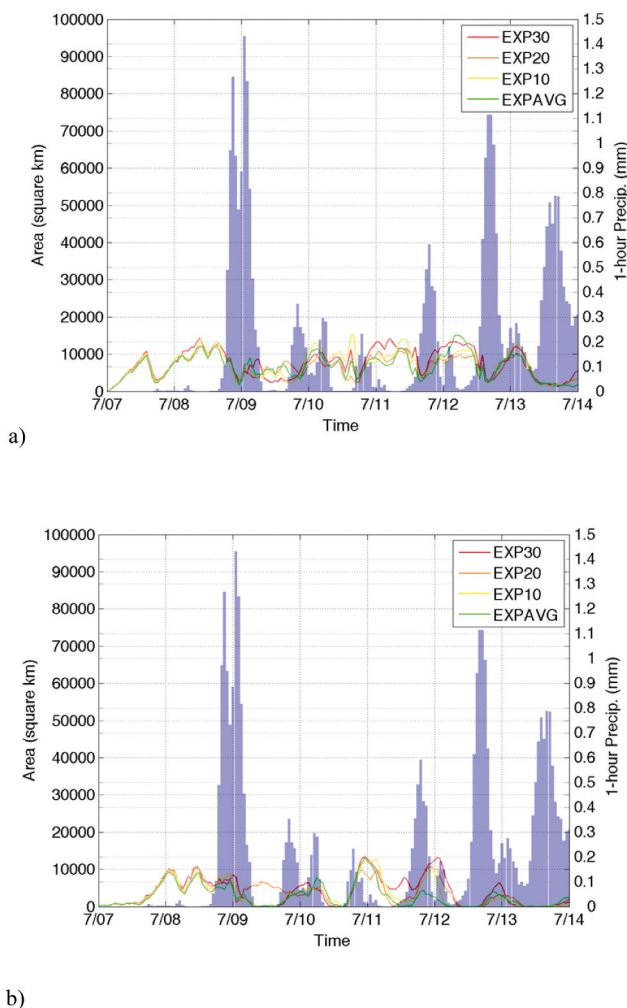


Figure 16. a) The area (km^2) of the vicinity of the CAFO emission locations with SO_2 concentrations exceeding 100 pptv above CTRL at the surface throughout the period in all EXP simulations (colored lines) and the area-averaged hourly precipitation for the same area in CTRL (blue bars). Dates represent 0000 UTC. b) Same as “a)” but for 850 mb.

aerosols. Previously, from observational data, Thornton et al. (2002) found higher concentration of SO_2 in the lower 1000 m and rapid decline above this altitude. These observations are similar to the findings by Ukhov et al. (2020) for different regions of the Middle East. During a multi-year WRF-Chem based simulations for the northern China Plains Liu et al. (2018) found that reduction in SO_2 emission is responsible for increased NH_3 . They have demonstrated that reduction in sulfate formation led to significant weakening of ammonium sulfate formation and increased in gas phase NH_3 formation. From a subcontinental-scale applications of WRF-Chem over east Asia, Zhong et al.

(2016) found that accuracy of SO₂ simulations varies from region to region and are season dependent.

In short, the WRF-Chem based simulated results related to vertical distribution and the nature of dispersion of SO₂ in our study are comparable to other studies. From the above discussions it is also evident that a vast majority of the SO₂ emission related studies were focused on its large-scale dispersions and in some cases its interactions with other chemical species. These findings apply to both observational data- and model-based research. In addition, almost none of these research were focused on agricultural emissions. In other words, our study is an important step for further applications of the WRF-Chem model for agricultural and specifically for SO₂ emissions from CAFOs and its local and regional dispersions.

Conclusions

Air pollution is well known for negatively impacting human health. These impacts include cardiovascular and respiratory health. In this context, the objective of this research was to simulate and analyze dispersion of the SO₂ emissions from CAFOs during wet and dry periods. In this study, SO₂ dispersions were analyzed horizontally and vertically during a one-week period that includes both wet and dry periods in July 2012. Due to the chemical reaction of SO₂ with water vapor, the assumption was that the presence of precipitation over the emission locations would result in changes to atmospheric concentration of SO₂ in their vicinity, and that the geographic spread of emissions would change during precipitation in comparison to drier conditions. A control simulation and four emissions change (experiment or EXP) simulations (each were 7 days long) were performed using the WRF-Chem model. SO₂ emissions at these locations were increased in the EXP simulations and then compared to the control simulation in order to isolate the simulated CAFO emissions from background SO₂. As noted previously, the length of the simulation is common in air pollution research (e. g., Loughner et al., 2011; Wang et al., 2011).

Lower-level SO₂ concentrations in the control simulation decreased to below 20 pptv with precipitation occurrence and increased to over 40 pptv during the drier periods following rainfall. This was likely due to the reaction of SO₂ with water and oxygen to form sulfuric acid (H₂SO₄) during rainy periods (Menz & Seip, 2004). Overall, background SO₂ concentrations tended to be greater at higher levels than those closer to the surface, and one contributing factor is the presence of liquid precipitation reacting with SO₂ in the lower levels. Concentrations of SO₂ in the upper levels over dry areas reached up to 100 pptv, while those over precipitation ranged between 0 and 30 pptv.

When emissions were increased from the control simulation in successive experimental simulations, increased SO₂ concentrations spread much farther from the CAFO emissions locations before and after precipitation. In most cases, however, the higher increases in SO₂ stayed limited to an area within a few kilometers of the emission sources. Exceptions to this occurred when lower-level wind speeds in the vicinity were greater, causing these high concentrations to travel farther from their sources before being influenced by other factors. Beyond the emission source locations, any increases in SO₂ concentrations above CTRL were mostly under 300

pptv. Wind direction was the main controlling factor in determining the areas of increased concentrations at any given time, especially during drier conditions, which allowed SO₂ to persist for longer periods.

This research can be improved and expanded in several ways. For instance, the simulation period used in this study extended over seven days. However, many of the major changes in SO₂ concentrations observed between dry and wet periods occurred within the first four days. With this in mind, future simulations of this kind can have a shorter duration and, therefore, save considerable computational resources. CAFOs primarily emit reduced sulfur compounds that convert to SO₂ in the atmosphere. Hydrogen sulfide (H₂S) is the most common of these and can yield SO₂ through atmospheric photochemical oxidation. Additional simulations using H₂S during the same period can be compared to the preceding SO₂ simulations in order to find a secondary relationship beyond that with precipitation occurrence. Future activities may also include observations of H₂S and use these data for the modeling research and verification.

Moreover, the methods used in this research can be applied to other locations and under different meteorological conditions. These emission simulations contribute to the research completed in other studies that have focused on CAFO emissions (Loughrin et al., 2011; Quintanar et al., 2013), which showed that the impacts of CAFOs on air quality and warrant attention due to the population that live near these operations.

Acknowledgments

The authors would like to thank two anonymous reviewers and the Associate Editor (Dr. Steven Quiring) for their valuable comments and suggestions which helped to improve this paper. Authors gratefully acknowledge feedback provided by Dr. Udaysankar Nair for an earlier version of this paper. The mention of any specific product names in this paper does not imply endorsement by the USDA.

Disclosure statement

No potential conflict of interest was reported by the authors.

Funding

Jesse Winchester, Rezaul Mahmood, and William Rodgers received funding from the USDA-ARS [Grant # 58-6445-6-068] to conduct this research. Rezaul Mahmood also acknowledges support from an NSF-ATM Chemistry Grant #1460418.

ORCID

William Rodgers  <http://orcid.org/0000-0001-5291-9471>

References

- Ackermann, I. J., Hass, H., Memmesheimer, M., Ebel, A., Binkowski, F. S., & Shankar, U. (1998). Modal aerosol dynamics model for Europe: Development and first applications. *Atmospheric Environment*, 32(17), 2981–2999. [https://doi.org/10.1016/S1352-2310\(98\)00006-5](https://doi.org/10.1016/S1352-2310(98)00006-5)
- AHPS (Advanced Hydrologic Prediction Service). (2012). *CONUS + Puerto Rico: Current 1-day observed precipitation, data from July 7 to 13, 2012, 1200 UTC*. NOAA. <http://water.weather.gov/precip/save.php?>
- Battye, W., Aneja, V., & Roelle, P. (2003). Evaluation and improvement of ammonia emissions inventories. *Atmospheric Environment*, 37(27), 3873–3883. [https://doi.org/10.1016/S1352-2310\(03\)00343-1](https://doi.org/10.1016/S1352-2310(03)00343-1)
- Bela, M. M., Barth, M. C., Toon, O. B., Fried, A., Homeyer, C. R., Morrison, H., Cummings, K. A., Li, Y., Pickering, K. E., Allen, D. J., Yang, Q., Wennberg, P. O., Crouse, J. D., St. Clair, J. M., Teng, A. P., O’Sullivan, D., Huey, L. G., Chen, D., Liu, X., Blake, D. R., . . . Diskin, G. (2016). Wet scavenging of soluble gases in DC3 deep convective storms using WRF-Chem simulations and aircraft observations wet scavenging of soluble gases in DC3 deep convective storms using WRF-Chem simulations and aircraft observations. *Journal of Geophysical Research Atmosphere*, 121, 4233–4257. <https://doi.org/10.1002/2015JD024623>
- Bernstein, D., Neelin, J., Li, Q., & Chen, D. (2012). Could aerosol emissions be used for regional heat wave mitigation? *Atmospheric Chemistry and Physics Discussions*, 12(9), 23793–23828. <https://doi.org/10.5194/acpd-12-23793-2012>
- Binkowski, F. S., & Shankar, U. (1995). The regional particulate matter model, 1. Mode description and preliminary results. *Journal of Geophysical Research*, 100(D12), 26191–26209. <https://doi.org/10.1029/95JD02093>
- Borlée, F., Yzermans, C. J., Aalders, B., Rooijackers, J., Krop, E., Maassen, C. B. M., Schellevis, F., Brunekreef, B., Heederik, D., & Smit, L. A. M. (2017). Air pollution from livestock farms is associated with airway obstruction in neighboring residents. *American Journal of Respiratory and Critical Care Medicine*, 196(9), 1152–1161. <https://doi.org/10.1164/rccm.201701-0021OC>
- Bunton, B., O’Shaughnessy, P., Fitzsimmons, S., Gering, J., Hoff, S., Lyngbye, M., Thome, P., Wasson, J., & Werner, M. (2007). Monitoring and modeling of emissions from concentrated animal feeding operations: Overview of methods. *Environmental Health Perspective*, 115(2), 303–307. <https://doi.org/10.1289/ehp.8838>
- Burkholder, J., Koplin, D., Koplin, D., Koplin, D., Thome, P., & Wichman, M. (2007). Impacts of waste from concentrated animal feeding operations on water quality. *Environmental Health Perspective*, 115(2), 308–312. <https://doi.org/10.1289/ehp.8839>
- Chapman, E., Gustafson, W., Jr., Easter, R., Barnard, J., Ghan, S., Pekour, M., & Fast, J. (2009). Coupling aerosol-cloud-radiative processes in the WRF-Chem model: Investigating the radiative impact of elevated point sources. *Atmospheric Chemistry and Physics*, 9(3), 945–964. <https://doi.org/10.5194/acp-9-945-2009>
- Chen, D., Liu, Z., Ban, J., & Chen, M. (2019). The 2015 and 2016 wintertime air pollution in China: SO₂ emission changes derived from a WRF-Chem/EnKF coupled data assimilation system. *Atmospheric Chemistry and Physics*, 19(13), 8619–8650. <https://doi.org/10.5194/acp-19-8619-2019>
- Chen, F., & Dudhia, J. (2001). Coupling an advanced land surface-hydrology model with the Penn State-NCAR MM5 modeling system. Part I: Model implementation and sensitivity. *Monthly Weather Review*, 129(4), 569–585. [https://doi.org/10.1175/1520-0493\(2001\)129<0569:CAALSH>2.0.CO;2](https://doi.org/10.1175/1520-0493(2001)129<0569:CAALSH>2.0.CO;2)
- Chuang, M.-T., Zhang, Y., & Kang, D. (2011). Application of WRF/Chem-MADRID for real-time air quality forecasting over the Southeastern United States. *Atmospheric Environment*, 45(34), 6241–6250. <https://doi.org/10.1016/j.atmosenv.2011.06.071>
- Cicerone, R., & Oremland, R. (1988). Biogeochemical aspects of atmospheric methane. *Global Biogeochemical Cycles*, 2, 299–332. <https://doi.org/10.1029/GB002i004p00299>
- Egan, S. D., Stauffer, M., Webley, P., Cahill, C. F., & Dean, J. (2014). WRF-Chem modeling of sulfur dioxide emissions from the 2008 Kasatochi Volcano. *Annals of Geophysics, Fast Track*, 2, 1–6. <https://doi.org/10.4401/ag-6626>

- EPA (Environmental Protection Agency). (2014). *Animal feeding operations*. EPA. <http://www.epa.gov/agriculture/anafoidx.html>
- Feilberg, A., Hansen, M. J., Liu, D., & Nyord, T. (2017). Contribution of livestock H₂S to total sulfur emissions in a region with intensive animal production. *Nature Communications*, 8(1), 1069. <https://doi.org/10.1038/s41467-017-01016-2>
- Freitas, S. R., Longo, K. M., Alonso, M. F., Pirre, M., Marecal, V., Grell, G., Stockler, R., Mello, R. F., & Gácita, M. S. (2011). PREP-CHEM-SRC – 1.0: A preprocessor of trace gas and aerosol emission fields for regional and global atmospheric chemistry models. *Geoscientific Model Development*, 4(2), 419–433. <https://doi.org/10.5194/gmd-4-419-2011>
- Gleason, J. F., Sinha, A., & Howard, C. J. (1987). Kinetics of the gas-phase reaction of HOSO₂ + O₂ → HO₂ + SO₃. *Journal of Physical Chemistry*, 91(3), 719–724. <https://doi.org/10.1021/j100287a045>
- Grell, G., Dudhia, J., & Stauffer, D. (1994). *A description of the fifth-generation Penn State/NCAR mesoscale model (MM5)* (NCAR Technical Note). Boulder, CO: NCAR. <http://nldr.library.ucar.edu/repository/assets/technotes/TECH-NOTE-000-000-000-214.pdf>
- Gross, A., & Stockwell, W. R. (2003). Comparison of the EMEP, RADM2 and RACM mechanisms. *Journal of Atmospheric Chemistry*, 44(2), 151–170. <https://doi.org/10.1023/A:1022483412112>
- Guenther, A., Karl, T., Harley, P., Wiedinmyer, C., Palmer, P., & Geron, C. (2006). Estimates of global terrestrial isoprene emissions using MEGAN (Model of emissions of gases and aerosols from nature). *Atmospheric Chemistry and Physics*, 6(11), 3181–3210. <https://doi.org/10.5194/acp-6-3181-2006>
- Hong, S.-Y., & Lim, J.-O. (2006). The WRF single-moment 6-class microphysics scheme (WSM6). *Journal of Korean Meteorological Society*, 42(2), 129–151.
- Hong, S.-Y., Noh, Y., & Dudhia, J. (2006). A new vertical diffusion package with an explicit treatment of entrainment processes. *Monthly Weather Review*, 134(9), 2318–2341. <https://doi.org/10.1175/MWR3199.1>
- Jiang, F., & Zhao, H. (2008). Numerical modeling of a continuous photochemical pollution episode in Hong Kong using WRF-chem. *Atmospheric Environment*, 42(38), 8717–8727. <https://doi.org/10.1016/j.atmosenv.2008.08.034>
- Jiang, X., Yang, Z., Liao, H., & Wiedinmyer, C. (2010). Sensitivity of biogenic secondary organic aerosols to future climate change at regional scales: An online coupled simulation. *Atmospheric Environment*, 44(38), 4891–4907. <https://doi.org/10.1016/j.atmosenv.2010.08.032>
- Kain, J., & Fritsch, J. (1993). Convective parameterization for mesoscale models: The Kain-Fritsch scheme. In K.A. Emanuel and D.J. Raymond (eds.) *The representation of cumulus convection in numerical models* (pp. 165–170). Boston, MA: American Meteorological Society.
- Karl, T., Apel, E., Hodzic, A., Riemer, D., Blake, D., & Wiedinmyer, C. (2009). Emissions of volatile organic compounds inferred from airborne flux measurements over a megacity. *Atmospheric Chemistry and Physics*, 9(1), 271–285. <https://doi.org/10.5194/acp-9-271-2009>
- Khan, R. R., & Siddiqui, M. J. A. (2014). Review on effects of particulates; sulfur dioxide and nitrogen dioxide on human health. *International Research Journal of Environment Sciences*, 3(4), 70–73.
- Khaniabadi, Y. O., Polosa, R., Chuturkova, R. Z., Daryanoosh, M., Goudarzi, G., Borgini, A., Tittarelli, A., Basiri, H., Armin, H., Nourmoradi, H., Babaei, A. A., & Naserian, P. (2017). Human health risk assessment due to ambient PM₁₀ and SO₂ by an air quality modeling technique. *Process Safety and Environmental Protection*, 111, 346–354. <https://doi.org/10.1016/j.psep.2017.07.018>
- Kim, Y., Sartelet, K., & Seigneur, C. (2011). Formation of secondary aerosols over Europe: Comparison of two gas-phase chemical mechanisms. *Atmospheric Chemistry and Physics*, 11(2), 583–598. <https://doi.org/10.5194/acp-11-583-2011>
- Kleinman, L., Daum, P., Imre, D., Lee, Y., Nunnermacker, L., & Springston, S. (2002). Ozone production rate and hydrocarbon reactivity in 5 urban areas: A cause of high ozone concentration in Houston. *Geophysical Research Letters*, 29(10), 1467–1470. <https://doi.org/10.1029/2001GL014569>

- Lee, S., Kim, S., Trainer, M., Frost, G., McKeen, S., Cooper, O., Flocke, F., Holloway, J., Neuman, J., Ryerson, T., Senff, C., Swanson, A., & Thompson, A. (2011). Modeling ozone plumes observed downwind of New York City over the North Atlantic Ocean during the ICARTT field campaign. *Atmospheric Chemistry and Physics*, 11, 7375–7397. <https://doi.org/10.5194/acp-11-7375-2011>
- Lin, M., Holloway, T., Carmichael, G., & Fiore, A. (2010). Quantifying pollution inflow and outflow over East Asia in spring with regional and global models. *Atmospheric Chemistry and Physics*, 10, 4221–4239. <https://doi.org/10.5194/acp-10-4221-2010>
- Liu, M., Huang, X., Song, Y., Xu, T., Wang, S., Wu, Z., Hu, M., Zhang, L., Zhang, Q., Pan, Y., Liu, X., & Zhu, T. (2018). Rapid SO₂ emission reductions significantly increase tropospheric ammonia concentrations over the North China plain. *Atmospheric Chemistry and Physics*, 18(24), 17933–17943. <https://doi.org/10.5194/acp-18-17933-2018>
- Loughner, C., Allen, D., Pickering, K., Zhang, D., Shou, Y., & Dickerson, R. (2011). Impact of fair-weather cumulus clouds and the Chesapeake Bay breeze on pollutant transport and transformation. *Atmospheric Environment*, 45(24), 4060–4072. <https://doi.org/10.1016/j.atmosenv.2011.04.003>
- Loughrin, J., Quintanar, A., Lovanh, N., & Mahmood, R. (2011). Heat flux measurements and modeling of malodorous compounds above an anaerobic swine lagoon. *Water, Air, and Soil Pollution*, 217(1–4), 463–471. <https://doi.org/10.1007/s11270-010-0601-z>
- Margitan, J. J. (1984). The mechanism of the atmospheric oxidation of sulfur dioxide, catalysis by OH. *Journal of Physical Chemistry*, 8(15), 3314–3318. <https://doi.org/10.1021/j150659a035>
- Meagher, J. F., Olszyna, K. J., & Luria, M. (1984). The effect of SO₂ gas phase oxidation on hydroxyl smog chemistry. *Atmospheric Environment*, 18(10), 2095–2104. [https://doi.org/10.1016/0004-6981\(84\)90195-1](https://doi.org/10.1016/0004-6981(84)90195-1)
- Menz, F., & Seip, H. (2004). Acid rain in Europe and the United States: An update. *Environmental Science and Policy*, 7(4), 253–265. <https://doi.org/10.1016/j.envsci.2004.05.005>
- Mesinger, F., DiMego, G., Kalnay, E., Mitchell, K., Shafran, P., Ebisuzaki, W., Jovic, D., Woollen, J., Rogers, E., Berbery, E., Ek, M., Fan, Y., Grumbine, R., Higgins, W., Li, H., Lin, Y., Manikin, G., Parrish, D., & Shi, W. (2006). North American regional reanalysis. *Bulletin of the American Meteorological Society*, 87(3), 343–360. <https://doi.org/10.1175/BAMS-87-3-343>
- Mlawer, E., Steven, J., Taubman, J., Brown, P., Iacono, M., & Clough, S. (1997). Radiative transfer for inhomogeneous atmospheres: RRTM, a validated correlated-k model for the longwave. *Journal of Geophysical Research*, 102(D-14), 16666–16682. <https://doi.org/10.1029/97JD00237>
- Mnatzaganian, C. L., Pellegrin, K. L., Miyamura, J., Valencia, D., & Pang, L. (2015). Association between sugar cane burning and acute respiratory illness on the island of Maui. *Environment and Health*, 14(1), 81. <https://doi.org/10.1186/s12940-015-0067-y>
- Mosier, A., Kroeze, C., Nevison, C., Oenema, O., Seitzinger, S., & van Cleemput, O. (1998). Closing the global N₂O budget: Nitrous oxide emissions through the agricultural nitrogen cycle. *Nutrient Cycling in Agroecosystems*, 52(2/3), 225–248. <https://doi.org/10.1023/A:1009740530221>
- National Research Council. (2003). *Air emissions from animal feeding operations: Current knowledge, future needs*. The National Academies Press.
- NCAR (National Center for Atmospheric Research). (2013). *WRF model various downloads*. NCAR. <http://www.mmm.ucar.edu/wrf/users/downloads.html>
- Ni, J.-Q., Robarge, W. P., Xiao, C., & Heber, A. J. (2012). Volatile organic compounds at swine facilities: A critical review. *Chemosphere*, 89(7), 769–788. <https://doi.org/10.1016/j.chemosphere.2012.04.061>
- Niemeier, U., Richter, J. H., & Tilmes, S. (2020). Differing responses of the quasi-biennial oscillation to artificial SO₂ injections in two global models. *Atmospheric Chemistry and Physics*, 20(14), 8975–8987. <https://doi.org/10.5194/acp-20-8975-2020>
- Ntelekos, A., Smith, J., Donner, L., Fast, J., Gustafson, W., Jr., Chapman, E., & Krajewski, W. (2009). The effects of aerosols on intense convective precipitation in the northeastern United States. *Quarterly Journal of the Royal Meteorological Society*, 135(643), 1367–1391. <https://doi.org/10.1002/qj.476>

- Perraud, V., Hone, J. R., Martinez, A. S., Kalinowski, J., Meinardi, S., Dawson, M. L., Wingen, L. M., Dabdub, D., Blake, D. R., Gerber, R. B., & Finlayson-Pitts, B. J. (2015). The future of airborne sulfur-containing particles in the absence of fossil fuel sulfur dioxide emissions. *Proceedings of the National Academy of Sciences*, 112(44), 13514–13519. <https://doi.org/10.1073/pnas.1510743112>
- Pope, C., III, Dockery, D., Spengler, J., & Raizenne, M. (1991). Respiratory health and PM₁₀ pollution: A daily time series analysis. *American Review of Respiratory Disease*, 144(3_pt_1), 668–674. https://doi.org/10.1164/ajrccm/144.3_Pt_1.668
- Pope, C. A., III, & Dockery, D. W. (2006). Health effects of fine particulate air pollution: Lines that connect. *Journal of the Air & Waste Management Association*, 56(6), 709–742. <https://doi.org/10.1080/10473289.2006.10464485>.
- Quintanar, A., Mahmood, R., Lovanh, N., Rawley, J., Becerra-Acosta, E., & Loughrin, L. (2013). Estimating greenhouse gas emissions from a waste lagoon. *Applied Engineering in Agriculture*, 29(4), 511–519. <http://dx.doi.org/10.13031/aea.29.10013>
- Rumsey, I., & Aneja, V. (2009, October 19–21). Measurement and modeling of emissions of reduced sulfur compounds from concentrated animal feeding operations. *Paper presented at the 8th Annual CMAS Conference*. Chapel Hill, NC.
- Saide, P., Carmichael, G., Spak, S., Gallardo, L., Osses, A., Mena-Carrasco, M., & Pagowski, M. (2011). Forecasting urban PM₁₀ and PM_{2.5} pollution episodes in very stable nocturnal conditions and complex terrain using WRF-Chem CO tracer model. *Atmospheric Environment*, 45(16), 2769–2780. <https://doi.org/10.1016/j.atmosenv.2011.02.001>
- Schell, B., Ackermann, I. J., Hass, H., Binkowski, F. S., & Ebel, A. (2001). Modeling the formation of secondary organic aerosol within a comprehensive air quality model system. *Journal of Geophysical Research: Atmospheres*, 106(D22), 28275–28293. <https://doi.org/10.1029/2001JD000384>
- Sigurdarson, S., & Kline, J. (2006). School proximity to concentrated animal feeding operations and prevalence of asthma in students. *Chest*, 129(6), 1486–1491. <https://doi.org/10.1378/chest.129.6.1486>
- Stockwell, W. R., Middleton, P., Chang, J., & Tang, X. (1990). The second generation regional acid deposition model chemical mechanism for regional air quality modeling. *Journal of Geophysical Research*, 16(343–16), 367. <https://doi.org/10.1029/JD095iD10p16343>
- Thornton, D. C., Bandy, A. R., & Blomquist, B. W. (1997). Transport of sulfur dioxide from the Asian Pacific rim to the North Pacific troposphere. *Journal of Geophysical Research*, 102(28), 489–28,499. <https://doi.org/10.1029/97JD01818>
- Thornton, D. C., Bandy, A. R., Blomquist, B. W., Davis, D. D., & Talbot, R. W. (1996). Sulfur dioxide as a source of condensation nuclei in the upper troposphere of the Pacific Ocean. *Journal of Geophysical Research*, 101(D1), 1883–1890. <https://doi.org/10.1029/95JD02273>
- Thornton, D. C., Bandy, A. R., Tu, F. H., Blomquist, B. W., Mitchell, G. M., Nadler, W., & Lenschow, D. H. (2002). Fast airborne sulfur dioxide measurements by atmospheric pressure ionization mass spectrometry (APIMS). *Journal of Geophysical Research*, 107(D22) 4632. <https://doi.org/10.1029/2002JD002289>
- Tie, X., Madronich, S., Li, G., Ying, Z., Zhang, R., Garcia, A., Lee-Taylor, J., & Liu, Y. (2007). Characterizations of chemical oxidants in Mexico City: A regional chemical dynamical model (WRF-Chem) study. *Atmospheric Environment*, 41(9), 1989–2008. <https://doi.org/10.1016/j.atmosenv.2006.10.053>
- Tu, F. H., Thornton, D. C., Bandy, A. R., Carmichael, G. R., Tang, Y., Thornhill, K. L., Sachse, G. W., & Blake, D. R. (2004). Long-range transport of sulfur dioxide in the central pacific. *Journal of Geophysical Research*, 109(D15), D15S08. <https://doi.org/doi:10.1029/2003JD004309>.
- Ukhov, A., Mostamandi, S., Krotkov, N., Flemming, J., da Silva, A., Li, C., Fioletov, V., McLinden, C., Anisimov, A., Alshehri, Y. M., & Stenchikov, G. (2020). Study of SO₂ pollution in the Middle East using MERRA-2, CAMS data assimilation products, and high-resolution WRF-Chem simulations. *Journal of Geophysical Research: Atmospheres*, 125, e2019JD031993. <https://doi.org/10.1029/2019JD031993>

- USDA (United States Department of Agriculture). (2013). *Animal feeding operations (AFO) and concentrated animal feeding operations (CAFO)*. USDA. <http://www.nrcs.usda.gov/wps/portal/nrcs/main/national/plantsanimals/livestock/afo/>
- Wang, M., Zhu, T., Zhang, J. P., Zhang, Q. H., Lin, W. W., Li, Y., & Wang, Z. F. (2011). Using a mobile laboratory to characterize the distribution and transport of sulfur dioxide in and around Beijing. *Atmospheric Chemistry and Physics*, 11(22), 11631–11645. <https://doi.org/10.5194/acp-11-11631-2011>
- Wang, X., Liang, X., Jiang, W., Tao, Z., Wang, J., Liu, H., Han, Z., Liu, S., Zhang, Y., Grell, G., & Peckham, S. (2010). WRF-Chem simulation of East Asian air quality: Sensitivity to temporal and vertical emissions distributions. *Atmospheric Environment*, 44(5), 660–669. <https://doi.org/10.1016/j.atmosenv.2009.11.011>
- Wilczak, J., McKeen, S., Djalalova, I., Grell, G., Peckham, S., Gong, W., Bouchet, V., Moffet, R., McHenry, J., McQueen, J., Lee, P., Tang, Y., & Carmichael, G. (2006). Bias-corrected ensemble and probabilistic forecasts of surface ozone over eastern North America during the summer of 2004. *Journal of Geophysical Research*, 111(D-23), 2156–2202. <https://doi.org/10.1029/2006JD007598>
- Winchester, J. (2015). *Emissions from concentrated animal feeding operations during wet and dry periods in the Southeastern United States* [Master's Thesis]. Western Kentucky University.
- Winkel, A., Mosquera, J., Groot Koerkamp, P. W. G., Ogink, N. W. M., & Aarnink, A. J. A. (2015). Emissions of particulate matter from animal houses in the Netherlands. *Atmospheric Environment*, 111, 202–212. <https://doi.org/10.1016/j.atmosenv.2015.03.047>
- Wu, Z., Wang, X., Chen, F., Turnipseed, A., Guenther, A., Niyogi, D., Charusombat, U., Xia, B., Munger, J., & Alapaty, K. (2011). Evaluating the calculated dry deposition velocities of reactive nitrogen oxides and ozone from two community models over a temperate deciduous forest. *Atmospheric Environment*, 45(16), 2663–2674. <https://doi.org/10.1016/j.atmosenv.2011.02.063>
- Yerramilli, A., Srinivas, C., Dasari, H., Tuluri, F., White, L., Baham, J., Young, J., Hughes, R., Patrick, C., Hardy, M., & Swanier, S. (2009). Simulation of atmospheric dispersion of elevated releases from point sources in Mississippi Gulf Coast with different meteorological data. *International Journal of Environmental Research and Public Health*, 6(3), 1055–1074. <https://doi.org/10.3390/ijerph6031055>
- Zhang, Y., Wen, X., & Jang, C. (2010). Simulating chemistry-aerosol-cloud-radiation- climate feedbacks over the continental U.S. using the online-coupled weather research forecasting model with chemistry (WRF/Chem). *Atmospheric Environment*, 44(29), 3568–3582. <https://doi.org/10.1016/j.atmosenv.2010.05.056>
- Zhang, Y., Zhu, Z., Zheng, Y., Chen, Y., Yin, F., Zhang, W., Dong, H., & Xin, H. (2019). Characterization of volatile organic compound (VOC) emissions from swine manure biogas digestate storage. *Atmosphere*, 10(7), 411. <https://doi.org/doi:10.3390/atmos10070411>.
- Zhong, M., Saikawa, E., Liu, Y., Naik, V., Horowitz, L. W., Takigawa, M., Zhao, Y., Neng-Huei, L., & Stone, E. A. (2016). Air quality modeling with WRF-Chem v3.5 in East Asia: Sensitivity to emissions and evaluation of simulated air quality. *Geoscientific Model Development*, 9(3), 1201–1218. <https://doi.org/10.5194/gmd-9-1201-2016>